UNCLASSIFIED
SECURITY CLASSIFICATION OF THIS PAGE

REPORT DOCUMENTATION PAGE

1a. REPORT SECURITY CLASSIFICATION: Unclassified	1b. RESTRICTIVE MARKINGS
2a. SECURITY CLASSIFICATION AUTHORITY	3. DISTRIBUTION/AVAILABILITY OF REPORT: Approved for public release; distribution unlimited.
2b. DECL	
4. PERFO **AD-A228 802**	5. MONITORING ORGANIZATION REPORT NUMBER(S): ARO 23956.6-G
6a. NAME OF PERFORMING ORGANIZATION: The University of Texas at Arlington; 6b. OFFICE SYMBOL (If applicable)	7a. NAME OF MONITORING ORGANIZATION: U. S. Army Research Office
6c. ADDRESS (City, State, and ZIP Code): Arlington, Texas 76019	7b. ADDRESS (City, State, and ZIP Code): P. O. Box 12211 Research Triangle Park, NC 27709-2211
8a. NAME OF FUNDING/SPONSORING ORGANIZATION: U. S. Army Research Office; 8b. OFFICE SYMBOL (If applicable)	9. PROCUREMENT INSTRUMENT IDENTIFICATION NUMBER: DAAL03-86-K-0149
8c. ADDRESS (City, State, and ZIP Code): P. O. Box 12211 Research Triangle Park, NC 27709-2211	10. SOURCE OF FUNDING NUMBERS: PROGRAM ELEMENT NO. / PROJECT NO. / TASK NO. / WORK UNIT ACCESSION NO.

11. TITLE (Include Security Classification)
VISUALIZATION OF UNSTEADY TRANSONIC FLOW BY HOLOGRAPHIC INTERFEROMETRY USING PHOTOREFRACTIVE MEDIA. (unclassified)

12. PERSONAL AUTHOR(S)
MAGNUSSON, ROBERT and WILSON, DONALD R.

13a. TYPE OF REPORT	13b. TIME COVERED	14. DATE OF REPORT (Year, Month, Day)	15. PAGE COUNT
FINAL	FROM 86/7/1 TO 90/6/30	90/8/31	32

16. SUPPLEMENTARY NOTATION
The view, opinions and/or findings contained in this report are those of the author(s) and should not be construed as an official Department of the Army position, policy, or decision, unless so designated by other documentation.

17. COSATI CODES		
FIELD	GROUP	SUB-GROUP

18. SUBJECT TERMS (Continue on reverse if necessary and identify by block number)
HOLOGRAPHIC INTERFEROMETRY, PHOTOREFRACTIVE MATERIALS, TRANSONIC AERODYNAMICS.

19. ABSTRACT (Continue on reverse if necessary and identify by block number)

This report summarizes results of research that was conducted to quantify the applicability of photorefractive media in holographic interferometry with emphasis on the visualization of unsteady aerodynamic transonic flow. The work was undertaken on the premise that photorefractive crystals possess properties that make them well suited for such applications. These properties include self-development, large data storage capacity via volume superposition, high sensitivity and resolution, erasability and reusability, real-time recording and readout, hologram fixing, and sensitivity to the recording light only. A broad range of experiments to parametrically quantify the use of iron-doped lithium niobate crystals for holographic interferometry was performed. High quality interferograms of

20. DISTRIBUTION/AVAILABILITY OF ABSTRACT	21. ABSTRACT SECURITY CLASSIFICATION
☐ UNCLASSIFIED/UNLIMITED ☐ SAME AS RPT. ☐ DTIC USERS	Unclassified
22a. NAME OF RESPONSIBLE INDIVIDUAL	22b. TELEPHONE (Include Area Code) / 22c. OFFICE SYMBOL

19 (continued)

nozzle discharge, airflow over airfoil, heat flux from electronic chips, and standing acoustic waves were produced. Archival storage by volume superposition was implemented to store a number of the Fourier transform double-exposure holograms that are used to produce the output interferograms. Sequences of flow-scenes were thus recorded and stored in a small fraction of the crystal volume. Experiments on thermal fixing of holograms in lithium niobate crystals were conducted and ionic, nonerasable holograms created. Real-time interferometry was implemented to use the high sensitivity of bismuth silicon oxide with fast response and short hologram lifetime. We conducted a basic study of the photocurrent response of these crystals as function of applied voltage and measured the useful diffraction efficiency obtainable without the application of an electric field. Interferometry by pulsed recording of holograms was then performed using an injection-seeded frequency-doubled Nd:YAG laser with a pulse length of 5 nanoseconds. Aerodynamic flow fields were recorded with turbulent flow clearly seen frozen in space by the short pulses. Asymmetric recording/readout characteristics of the double-exposure holograms were obtained by two-photon recording in doped and undoped crystals. The interferograms were low-noise and the rate of erasure slower than with single-photon gratings. Holographic subtraction interferometry was then performed and the quantitative dependence of the subtraction on the diffraction efficiency of the refractive-index grating measured. Example applications of coherent image subtraction in photorefractively generated interferograms were demonstrated. The final phase of the research was an evaluation of the interferometry system in the UTA transonic Ludwieg-tube wind tunnel. Photorefractive holograms were easily recorded with the pulsed laser during quiet conditions but with spatially noisy holograms resulting during tunnel firing. We speculate that this is caused by the extremely short exposure times of the Nd:YAG laser resulting in a snapshot of the instaneous turbulent fluctuations. The signals are thus buried in noise. Further tests are planned to clarify this point.

VISUALIZATION OF UNSTEADY TRANSONIC FLOW BY HOLOGRAPHIC INTERFEROMETRY USING PHOTOREFRACTIVE MEDIA

FINAL REPORT

Robert Magnusson and Donald R. Wilson

August 31 , 1990

U. S. Army Research Office

Grant DAAL03-86-K-0149

The University of Texas at Arlington

Approved for Public Release;
Distribution Unlimited

THE VIEW, OPTIONS, AND/OR FINDINGS CONTAINED IN THIS REPORT ARE THOSE OF THE AUTHORS AND SHOULD NOT BE CONSTRUED AS AN OFFICIAL DEPARTMENT OF THE ARMY POSITION, POLICY, OR DECISION UNLESS SO DESIGNATED BY OTHER DOCUMENTATION.

TABLE OF CONTENTS

1. PROBLEM STATEMENT

The primary objective of the proposed research was to quantify the applicability of photorefractive media in holographic interferometry as applied to the visualization of unsteady transonic flow. Photorefractive crystals possess properties that make them well suited for holographic interferometry applications. These properties include instantaneous hologram formation (self-development), huge data storage capacity via volume superposition (three-dimensional storage), high sensitivity and resolution, erasability and reusability, real-time recording and readout, hologram fixing (archival storage), and sensitivity to the recording light only. Photorefractive crystals will be important recording media in future holographic interferometry. For aerodynamics, heat transfer, acoustics, and other areas where a large number of interferograms must be rapidly recorded and processed, photorefractive materials have significant advantages over photographic film. ~~Accordingly,~~ this work's the focus ~~of the work~~ was to carry out a program of research and development to define in detail the applicability of photorefractive crystals to interferometry for the visualization of dynamic flow fields and to establish the techniques necessary for efficient utilization of such media. The concepts developed included volume hologram superposition, real-time interferometry, hologram fixing, coherent image subtraction, and asymmetric recording/readout hologram characteristics (two photon recording). The application of these concepts to the visualization of unsteady transonic flow-fields was emphasized.

2. SUMMARY OF RESULTS

2.1 Introduction

A total of 8 progress reports covering the period 1 July 1986-30 June 1990 have been submitted for this project. In addition, great many detailed results are reported in the theses of J. H. Mitchell III (M.S.E.E. 1987), A. Hafiz (M.S.E.E. 1989), and J. P. Englehardt (M.S.A.E. 1989). Some of these results have been reported in the literature and presented at conferences.

In this report, we will briefly summarize the main achievements of this research that have been previously reported. In a separate section, we will then in more detail describe recent, unreported results.

2.2 Summary of previous results

A. Parametric study of iron-doped lithium niobate crystals for interferometry.

A broad range of experiments to quantify the use of iron-doped lithium niobate for holographic interferometry has been performed. This includes experiments with crystals of various levels of iron doping and hologram recording in both reflection and transmission geometry (i.e. different orientations of the crystal optical axis). The crystals were repeatedly thermally erased (when full of holograms) and showed no fatigue. A variety of combination amplitude and phase objects or pure-phase objects have been visualized. Examples are nozzel discharge, airflow over airfoil, heat flux from electronic chips, and standing acoustic waves. Reconstructed interferograms have been compared with corresponding results using photographic film and comparable quality found.

B. Archival storage by volume superposition

Fourier transform double-exposure holography is used to produce the output interferograms. Thus, only very small spots (3-5 mm^2) on the crystals are needed. Additionally, since the holograms are Bragg volume holograms, strong angular selectivity exists. This allows volume superposition of holograms by angular multiplexing. We have recorded and stored 33 double-exposure holograms in the same crystal location (spot size ~ 5 mm^2) by 0.25° crystal rotation between exposures with negligible crosstalk. Over 100 such holograms could easily be stored. Sequences of flow-scenes are thus recorded and stored.

C. Thermal fixing of holograms

Experiments on thermal fixing of holograms in lithium niobate crystals were conducted. The idea is that first the reference scene is recorded and thermally fixed in the crystal. Then, in the same crystal volume, holograms of the (dynamic) flow-field of interest are

superimposed. The experiments showed only limited success and we believe that optical fixing techniques such as two-photon recording may be more useful.

D. Real-time interferometry in BSO

Real-time interferometry uses the high sensitivity obtainable in media such as bismuth silicon oxide (BSO) possessing fast response and thus short hologram lifetime. Holograms of the scenes to be compared are superimposed and the output interferogram is generated within the lifetime of the first hologram. We conducted a basic study of the photocurrent response of BSO crystals as function of applied voltage using a picoammeter, with results shown in Fig. 1. Short lifetime holograms (1 millisecond lifetime) were recorded with the argon laser. Diffraction efficiency of 0.2% was obtained without the application of an electric field across the crystal.

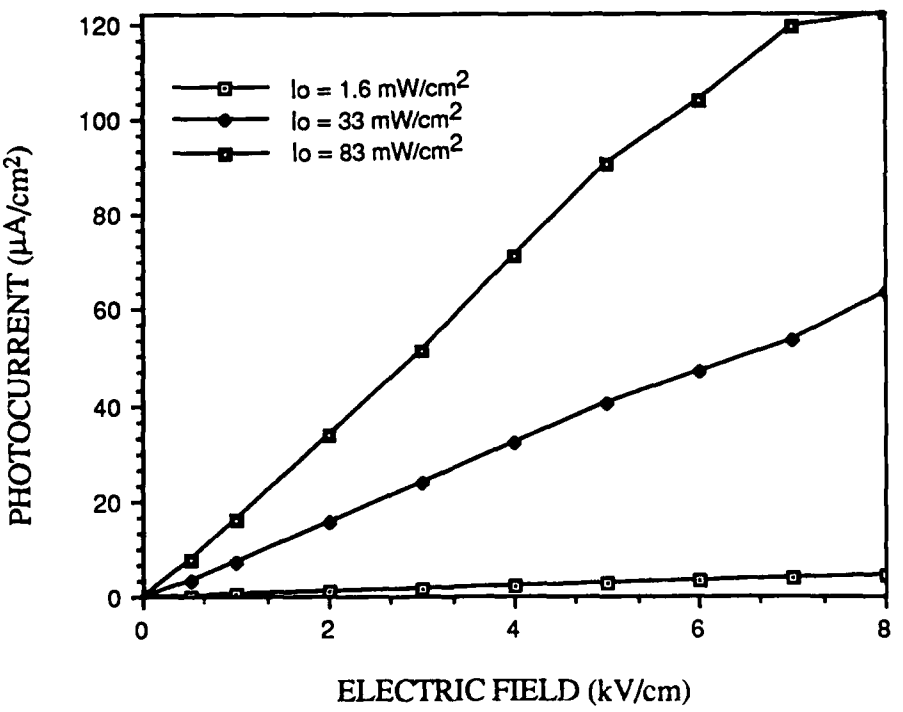

Figure 1 Photocurrent density in a BSO crystal as function of argon laser illumination (λ=0.514 μm) and applied electric field.

E. Interferometry by pulsed recording of holograms

For the pulsed experiments, a new injection-seeded frequency-doubled Nd:YAG pulsed laser system with a pulse length of 5 nanoseconds was installed. Both two- and three-dimensional aerodynamic flow fields were recorded. Turbulent flow was seen quite clearly, frozen in space by these short pulses. This initial phase was carried out with green light (the frequency-doubled component) only and using iron-doped lithium niobate crystals. Information retrieval was accomplished with a low power He-Ne laser or the recording Nd:YAG laser directly.

F. Asymmetric recording/readout by two-photon recording: Doped crystals

Using the two-photon technique with the Nd:YAG laser (i.e. both lines at 532 nm and 1064 nm simultaneously present), gives greatly improved results. The interferograms are noise-free and the sensitivity is significantly enhanced. In the iron-doped crystals, it was found that permanent fixing (i.e. not optically erasable) in these moderately sensitive materials does not occur since reading with a low power He-Ne laser erased the holograms gradually. However, the rate of erasure was much slower than with single-photon (532 nm only) gratings.

G. Asymmetric recording/ readout by two-photon recording: Undoped crystals

Undoped $LiNbO_3$ can be an effective storage material with the two-photon recording technique . Our experiments showed that whereas the dynamic range of the undoped crystals is rapidly (5-10 superimposed holograms) depleted using single-photon recording, the dynamic range of the crystal can be extended and controlled by the second beam of infrared light (i.e. two-photon recording). This is a very interesting result. Experiments with laser erasure and white light erasure of the two-photon holograms were then performed. In both cases, slow erasure was observed but with significantly extended lifetimes over the iron-doped crystal interferograms. The undoped crystals are much cheaper than iron-doped $LiNbO_3$.

2.3 Summary of recent results

A. Holographic subtraction interferometry

Subtraction of images can be accomplished holographically by introducing a π phase shift in the reference beam between the two exposures. Hariharan[2] and Trolinger[3] have demonstrated that holographic subtraction interferometry can work quite well. The procedure is to first record a hologram of a object in its initial condition and then record a superimposed hologram of the object in its final state with a π phase-shift in the reference beam. Reconstruction reveals that parts common to both objects have been erased. Guest et al.[4] have employed similar ideas for binary image subtraction in photorefractive crystals. Also, it has been demonstrated that any given hologram in a stack of angularly multiplexed holograms can be selectively erased.[5] We present in this section the dependence of the subtraction on the diffraction efficiency of the refractive index grating and the application of coherent image subtraction in photorefractively generated interferograms.

An argon-ion laser operating at 0.514 μm is used to write holograms in the lithium niobate (crystal size 10×10×2 mm^3, 0.05% iron doped). The beam is divided into the object beam and the reference beam with the reference beam passing through a phase modulator that can introduce a π phase shift. A He-Ne laser is used to monitor the diffracted power of the photorefractive index grating. Fig. 2 shows the measured diffraction efficiency during three different periods: At first the diffraction efficiency increases as a function of the exposure time, then it remains constant while the π phase shift is being made. The second exposure with the π phase shift produces a refractive index grating complementary to the grating resulting from the first hologram. Therefore, the diffraction efficiency drops from the peak level to a minimum value during the third period. The smaller this minimum value is, the better the substraction has worked. It is evident from Fig. 2 that lower diffraction efficiency is preferable.

The experimental arrangement for holographic subtraction interferometry is shown in Fig. 3, with example results shown in Figs. 4 and 5.

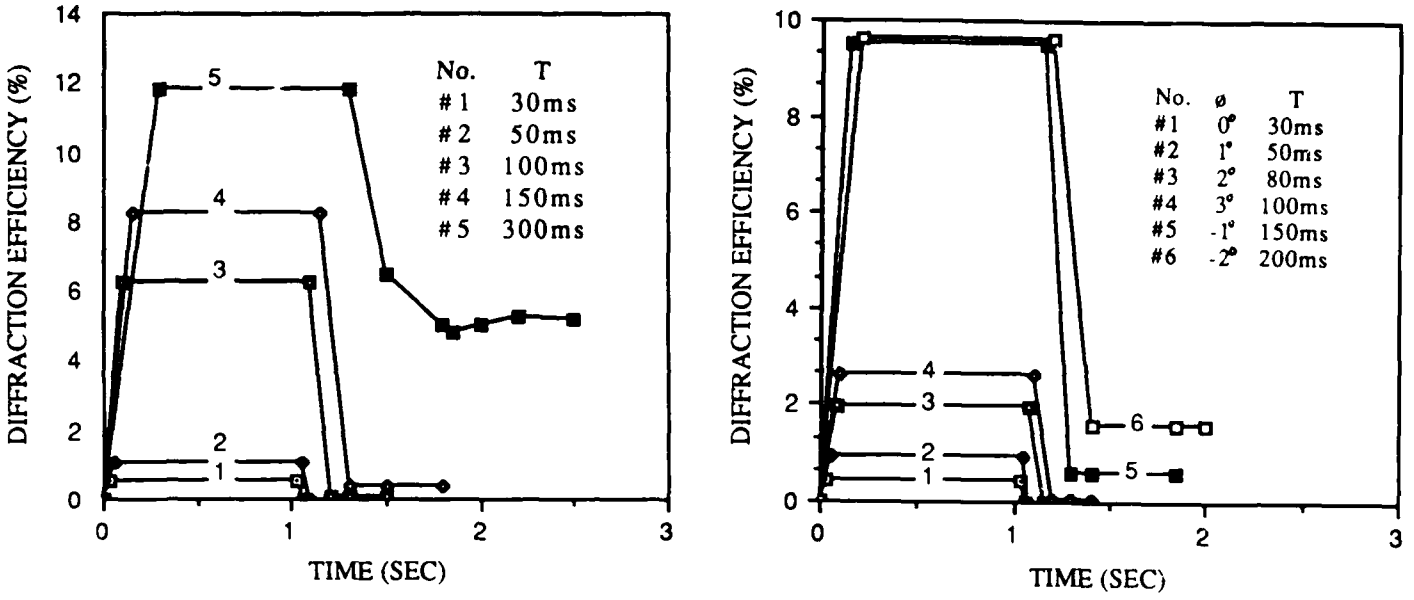

(a) (b)

Figure 2 Diffraction efficiency vs exposure time during the first exposure, followed by π phase shift and the second exposure: (a) holograms in different transverse crystal locations, (b) angularly multiplexed holograms. T is the hologram recording time and ϕ is the crystal rotation angle. The horizontal part of the curve is the arbitrary time-delay between the two expossures.

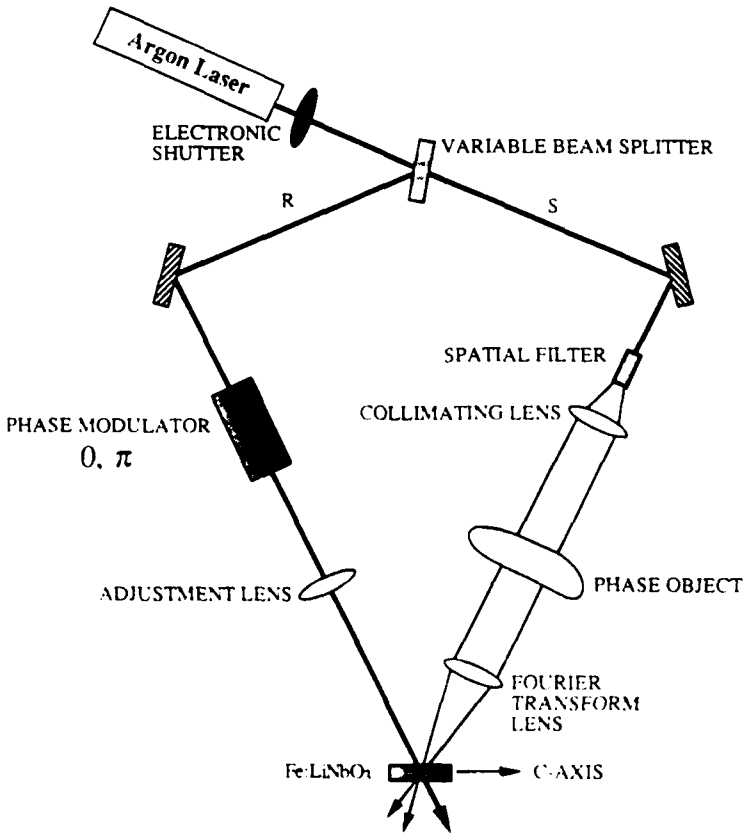

Figure 3 System for holographic subtraction interferometry.

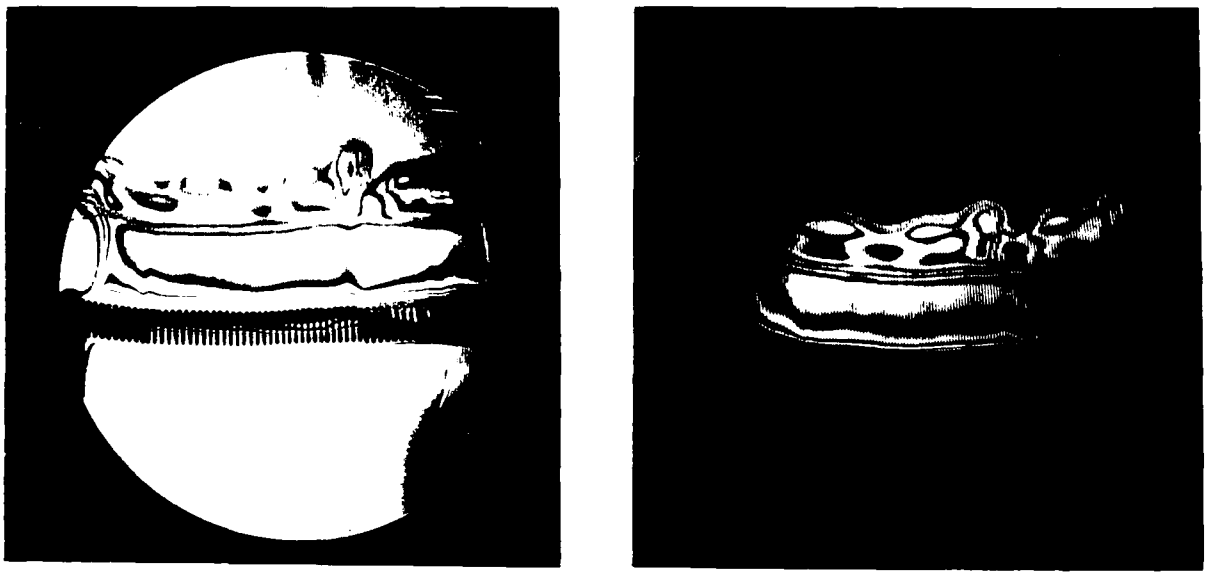

(a) (b)

Figure 4 Holographic subtraction interferometry: (a) without π phase shift between the two exposures, (b) with π phase shift between the two exposures and thus the background erased. The object is a heated coil.

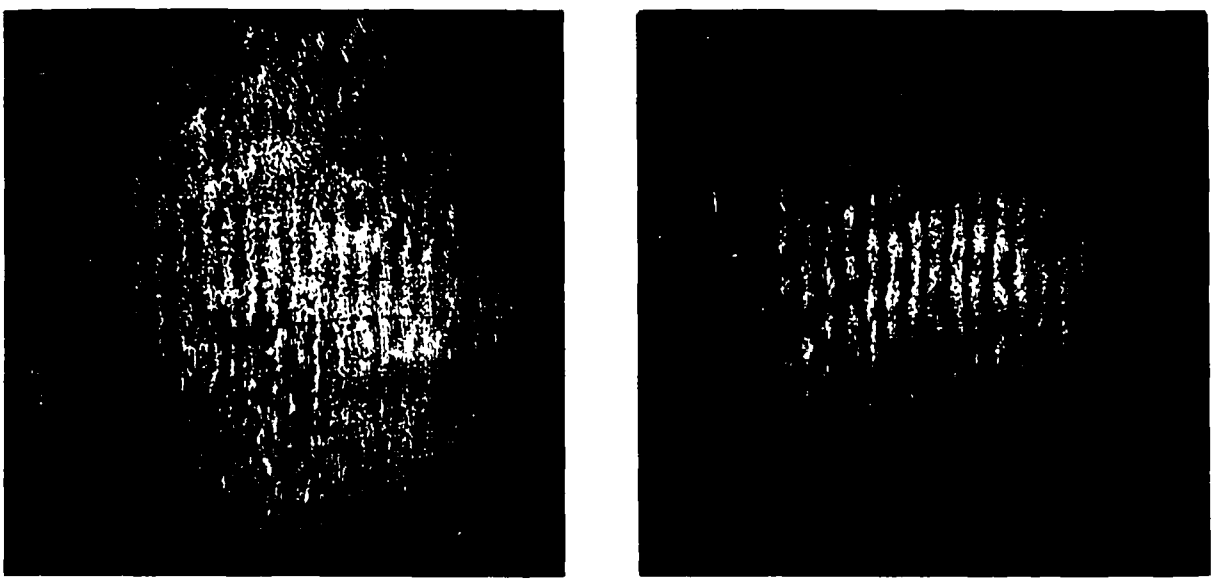

(a) (b)

Figure 5 Holographic subtraction interferometry: (a) without π phase shift between the two exposures, (b) with π phase shift between the two exposures and thus the background erased. The object is a standing acoustic wave in a water tank. Acoustic frequency is 450kHz and acoustic wavelength is 3.3 mm. The transducer is on the left.

In conclusion, photorefractive crystals can be used as the recording material in holographic subtraction interferometry. The diffraction efficiency of the hologram should be low to obtain a good subtraction. It must be noted that we did not use a phase stabilization system in our experiments. This system is required for objects that cause vibration during recording (such as in aerodynamics) and can be easily incorporated into the experiments.

B. Transonic tunnel test program

The final phase of the research program involved an evaluation of the interferometry system in the UTA transonic Ludwieg-tube wind tunnel[6]. The tunnel test section was modified to add optical windows in all four walls, at the axial location corresponding to the center of model rotation. Initially, three separate test evaluations of the pulsed interferometry system were planned. These tests were to be a duplication of previous tests conducted during the ARO-sponsored research program to investigate helicopter rotor blade-vortex interactions[7,8]. These tests included:

1. Visualization of the transonic flow over the basic NACA 0012 airfoil model used during the BVI test program.
2. Visualization of the perpendicular BVI interaction[7].
3. Visualization of the parallel BVI interaction[8].

Unfortunately, as a result of unanticipated problems, only the first two tests were conducted, and the results from these tests were generally disappointing.

The first test involved positioning the basic NACA 0012 airfoil in the optical window, and viewing the transonic flow development over the upper surface of the airfoil for a range of Mach numbers from 0.8 to 0.9. The optical system was aligned and a hologram of the no-flow background scene was successfully recorded. However, great difficulty was encountered in trying to record a hologram of the dynamic flow field, in that it appeared extremely turbulent. Initially, the problem was thought to be a result of mechanical or acoustical induced vibration of either the laser or optical system. A significant effort was made to provide both mechanical and acoustical isolation of the optical system, but no apparent improvement in the double-exposure interferograms was observed. A video system

was installed to monitor system stability and reference/object beam overlap during tunnel firing. This showed ample system stability for the work. Still, the resulting images appeared to be totally distorted, as if viewing a highly-turbulent flow field. An example pattern is shown in Fig. 6 as observed by directly recording the object wave passing through the tunnel by a video camera. Following up on this premise, a modification of the optical window system was introduced (i.e. internal optical windows added) to reduce the turbulence in the plenum cavity to keep it from distorting the optical beam. However, this too failed to significantly improve the optical image.

The next phase of the test program involved replacing the pulsed Nd:YAG laser with a cw He-Ne laser and recording shadowgraphs of the flow in an attempt to identify the cause of the problem. Recording of the shadowgraphs proved to be straightforward, and all of the expected details of the flowfield could easily be observed. For example, wave patterns emanating from slight surface irregularities associated with installation of the surface-mounted pressure transducers were clearly visible, as was the upper surface shock wave structure as shown in Fig. 7. Furthermore, aft movement and strengthening of the shock wave with increases in Mach number were clearly evident.

Following the successful shadowgraph recording for the basic airfoil, the next phase of the test program involved introducing a vortex generator upstream of the 0012 airfoil, and attempting to record the details of the perpendicular BVI. Again, attempts to record interferograms with the pulsed laser were unsuccessful, however, the details of the interaction were visible (see Fig. 8) in (videotaped) shadowgraphs taken with the cw laser. In general, the location and extent of the vortex appeared to agree with results from the earlier aerodynamic tests reported in Ref.7. At this point the test program was terminated. It was felt that attempts to record interferograms of the parallel BVI would be fruitless, and the optics for the cw laser experiment were not suited for recording the transient nature of the parallel BVI.

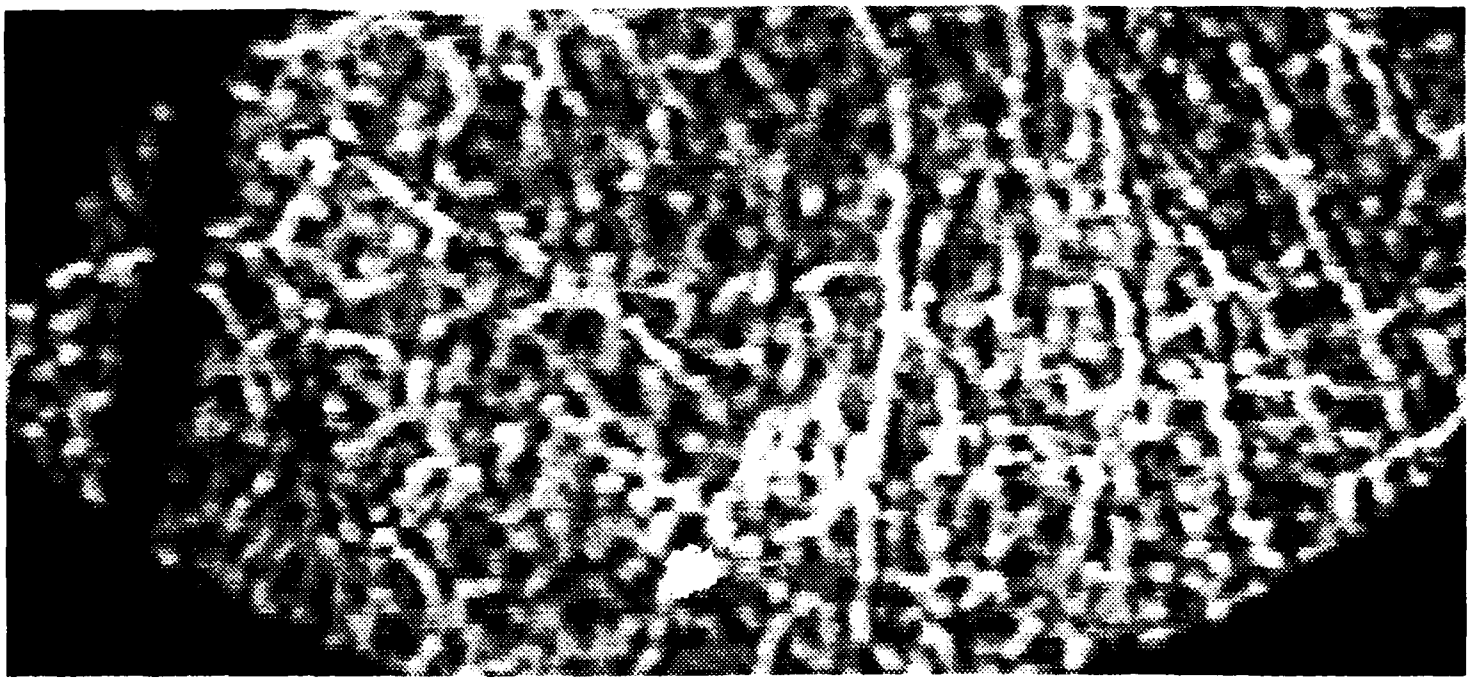

Figure 6 Aerodynamic turbulence in the wind tunnel during a run recorded using a video camera and a single expanded 5 nanosecond pulse from the Nd:YAG laser. Pressure in the Ludwieg tube before firing was 100 psi.

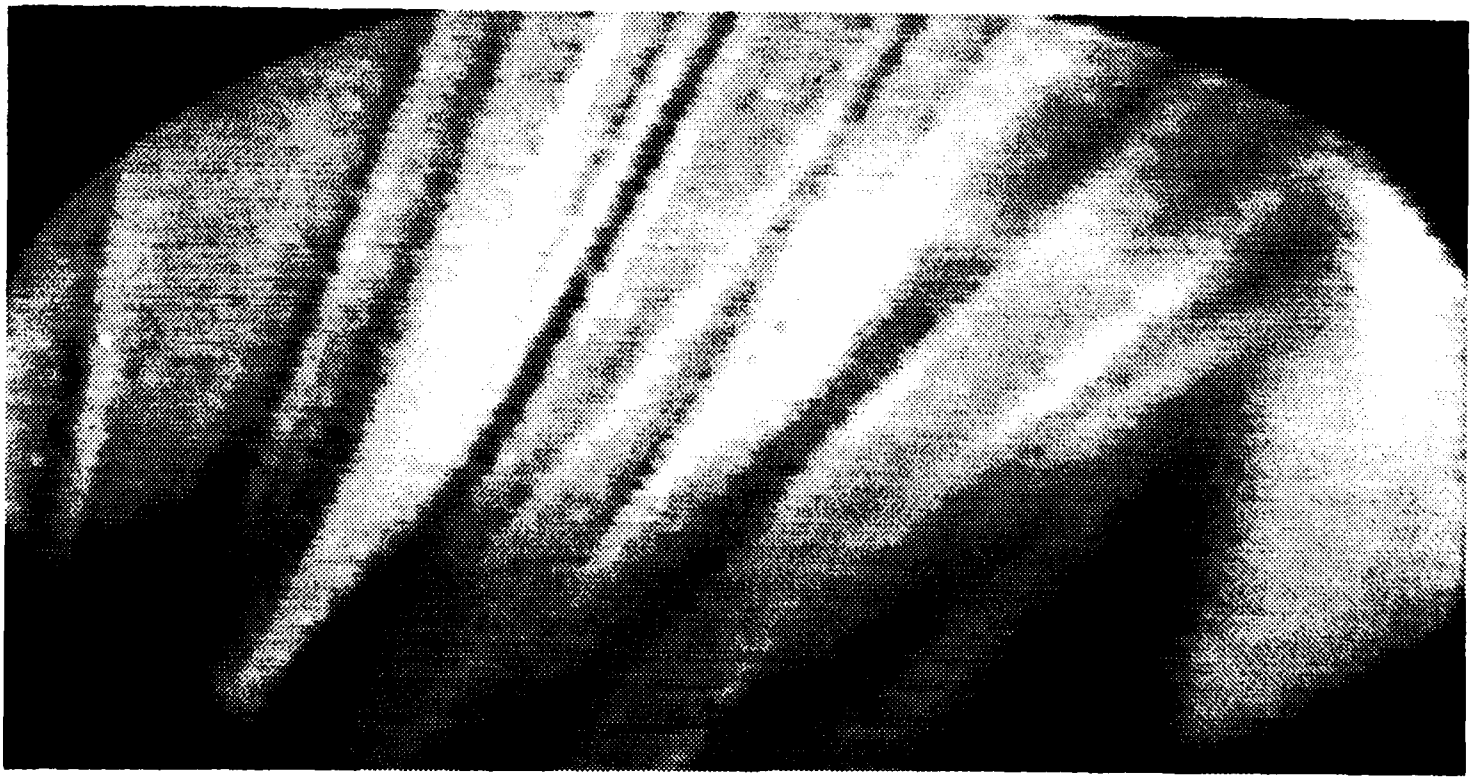

Figure 7 Shock wave structure visualized with a videocamera and a cw He-Ne laser. The airfoil is at the bottom of the figure and the flow is from the left.

Figure 8 Vortex structure visualized with a cw He-Ne laser and a videocamera. The flow is from the left.

The cause of the failure to obtain good interferograms with the pulsed laser system is not completely known. The most likely speculation is that the extremely short exposure times (5nsec) result in a "snapshot" of the instantaneous turbulent fluctuations. The integrated optical path for the laser beam through the test volume is 18.5 cm in the Ludwieg tube. For the small wind tunnel used in many of our proof-of-principle experiments, this path length was only 0.5 cm. In the latter case, the effects of turbulence were clearly seen but with the signal still retrievable. Similar results can also be observed in some of the flow visualization photographs shown in van Dyke's monogram (Ref. 9) that were taken with exposure times covering a number of orders of magnitude. For example, schlieren photographs of an underexpended jet taken at long exposures tend to clearly show the details of the shock and expansion waves, whereas photographs of the same flow with drastically reduced exposure times tend to show more of a chaotic flow corresponding to turbulent fluctuations. Similar

results were observed in our experiments involving pulsed and cw interferograms of the flow in a converging-diverging nozzle. Further tests are planned to explore this issue, and to see if these techniques have promise for the optical investigation of turbulent flowfields.

3. REFERENCES

1. A. M. Glass, "The photorefractive effect", Optical Engineering **17**, 470 (1978).
2. P. Hariharan, "Application of holographic subtraction to time-average hologram interferometry of vibrating objects," Applied Optics **12**, 143 (1973).
3. J. D. Trolinger, "Application of generalized phase control during reconstruction to flow visualization holography," Applied Optics **18**, 766 (1979).
4. G. C. Guest, M. M. Mirsalehi, and T. K. Gaylord, "EXCLUSIVE OR processing (binary image subtraction) using thick Fourier holograms," Applied Optics **23**, 2444 (1984).
5. J. P. Huignard, J. P. Herriau, and F. Micheron, "Coherent selective erasure of superimposed volume holograms in $LiNbO_3$," Applied Physics Letters **26**, 256 (1975).
6. D. R. Wilson and S. Y. Chou,, "Development of the UTA High Reynolds Number Transonic Wind Tunnel" AIAA Paper 85-0135, AIAA 23rd Aerospace Sciences Meeting, Reno, Nevada, January 14-17, 1985.
7. D. R. Wilson, I. M. Kalkhoran, and D. D. Seath, "An Experimental Investigation of the Perpendicular Vortex-Airfoil Interaction at Transonic Speeds," AIAA Paper 87-0208, AIAA 25th Aerospace Sciences Meeting, Reno, Nevada, January 12-15, 1987.
8. I. M. Kalkhoran, D. R. Wilson, and D. D. Seath, "An Experimental Investigation of the Parallel Vortex-Airfoil Interaction at Transonic Speeds," AIAA Paper 89-1833, AIAA 20th Fluid Dynamics, Plasmadynamics and Lasers Conference, Buffalo, New York, June 12-14, 1989.
9. M. Van Dyke, An Album of Fluid Motion, The Parabolic Press, Stanford, CA, 1982.

4. PUBLICATIONS

The following conference papers, theses, and journal articles were produced to document the research results of this program.

1. R. Magnusson, "Holographic interferometry in photorefractive crystals," 14th UTA-AIAA Mini-Symposium, March 1986.

2. J. H.Mitchell III, R. Magnusson, T. D. Black, D. R. Wilson, "Experimental holographic interferometry in iron-doped lithium niobate," 14th UTA-AIAA Mini-Symposium, March 1986.

3. J. H.Mitchell III, R. Magnusson, T. D.Black and D. R. Wilson, "Flow-field visualization by holographic interferometry in iron-doped lithium niobate crystals," Optical Society of America Annual Meeting, October 19-24, 1986.

4. J. H.Mitchell III, R. Magnusson, T. D. Black, and D. R. Wilson, "Use of self-developing optical crystals for visualization of flow-fields," 15th UTA-AIAA Mini-Symposium, February 1987.

5. R. Magnusson, J. H. Mitchell III, T. D. Black, D. R. Wilson, "Holographic interferometry using iron-doped lithium niobate," *Applied Physics Letters*, vol. 51, pp. 81-82, July 1987.

6. R. Magnusson, J. H.Mitchell III, T. D. Black, and D. R. Wilson, "Interferometry in lithium niobate crystals with fixed reference holograms," Optical Society of America Annual Meeting, October 18-23, 1987.

7. R. Magnusson, A. Hafiz, T. D. Black, and D. R. Wilson, "Interferometry based on holographic storage in optical crystals," IEEE MIDCON/88, August 30 - September 1, 1988.

8. A. Hafiz, R. Magnusson, D. R. Wilson, and T. D. Black, "Holographic interferometry using optical crystals," Optical Society of America Annual Meeting, October 31 - November 4, 1988.

9. A. Hafiz, R. Magnusson, J. S. Bagby, D. R. Wilson, and T. D. Black, "Visualization of aerodynamic flow fields using photorefractive crystals," *Applied Optics*, vol. 28, pp. 1521-1524, 15 April 1989.

10. A. Hafiz and R. Magnusson, "Interferometry using pulsed recording of holograms in lithium niobate", Optical Society of America Annual Meeting, October 15-20, 1989.

11. R. Magnusson and A. Hafiz, "Holographic interferometers based on self developing optical crystals," The 15th Congress of the International Commission for Optics "Optics in Complex Systems," August 5-10, 1990, Bavaria, Germany.

12. A. Hafiz, R. Magnusson, J. S. Bagby and A. Haji-Sheikh, "Holographic imaging of transient natural convection from electronic components," Heat Transfer Division of the American Society of Mechanical Engineers, 1990 Winter Annual Meeting, November 25-30, 1990, Dallas, Texas (accepted).

13. R. Magnusson, A. Hafiz, J. S. Bagby, and A. Haji-Sheikh, "Holographic interferometry using self-developing optical crystals for heat flux evaluation," to appear in the *Journal of Electronic Packaging*, December 1990.

14. J. H. Mitchell III, "Holographic interferometry in iron-doped lithium niobate crystals with application to visualization of unsteady transonic flow", M. S. Thesis, 1987.

15. A. M. Hafiz, "Experimental holographic interferometry using photorefractive crystals", M. S. Thesis, December 1989.

16. J. P. Engelhardt, "A transonic wind tunnel electronic control unit and total pressure survey of a vortex", M. S. Thesis, December 1989.

5. SCIENTIFIC PERSONNEL

Dr. R. Magnusson, Principal Investigator

Dr. D. R. Wilson, Principal Investigator

Mr. A. M. Hafiz, Graduate Research Assistant, M.S. E. E., December 1989

Mr. J. H. Mitchell III, Graduate Research Assistant, M.S. E. E., May 1987

Mr. J. K. Wong, Graduate Research Assistant

Mr. J. Joe, Undergraduate Research Assistant

Ms. M. Moghaddam, Undergraduate Research Assistant

Mr. J. P. Englehardt, Graduate Research Assistant, M. S. A. E., December 1989

Mr. W. S. Stuessy, Graduate Research Assistant

Mr. D. Bryant, Undergraduate Research Assistant

APPENDIX : SELECTED PUBLICATIONS

INTERFEROMETRY BASED ON HOLOGRAPHIC STORAGE IN OPTICAL CRYSTALS

R. Magnusson & A. Hafiz, Department of Electrical Engineering,
T. D. Black, Department of Physics,
D. R. Wilson, Department of Aerospace Engineering,
P. O. Box 19016, The University of Texas at Arlington
Arlington, Texas 76019

INTRODUCTION

Holographic interferometry is a well established technique for a wide variety of practical applications. This basic approach and its numerous variants are being increasingly employed in research and industry. In most of these cases, the recording medium used has been photographic film. This medium is quite satisfactory when relatively few exposures are to be recorded or when steady-state phenomena are under study. The use of film, however, may become extremely inconvenient when a large number of exposures is needed due to the tedium of film development. Thus, self-developing optical crystals may become the media of choice in future interferometry applications. It is the purpose of the present paper to describe research on holographic interferometry in self-developing (photorefractive) crystals and to present experimental results.The improvements brought about by these improved materials and procedures could potentially revolutionize the field of holographic interferometry.

PHOTOREFRACTIVE MATERIALS

Photorefractive crystals are promising recording media for many applications including holographic interferometry. The crystals are self-developing (instantaneous hologram formation), highly sensitive, eraseable, possess high resolution, and are reuseable. Very little research has been done on the applicability of this class of materials to interferometry.[1-5]

The basic process of hologram formation in, for example, $LiNbO_3$ can be described generally as follows: With the crystal placed at the intersection of two (interfering) laser beams, electrons are excited from traps within the bright fringes of the interference pattern. These electrons then migrate out of the bright fringes and are retrapped in the dark fringes. The resulting spatially varying charge distribution creates space-charge fields that modulate the refractive index of the crystal via the electro-optic effect. This spatially varying refractive

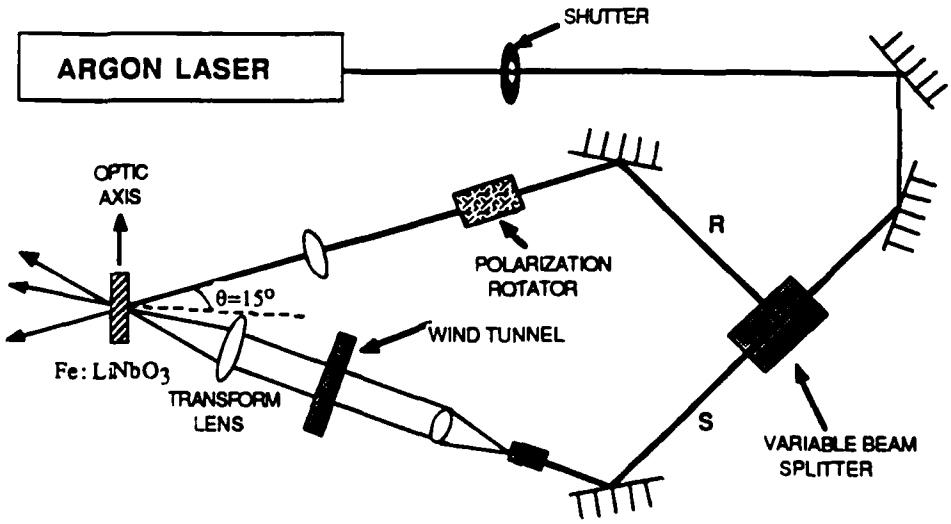

Figure 1 Experimental system.

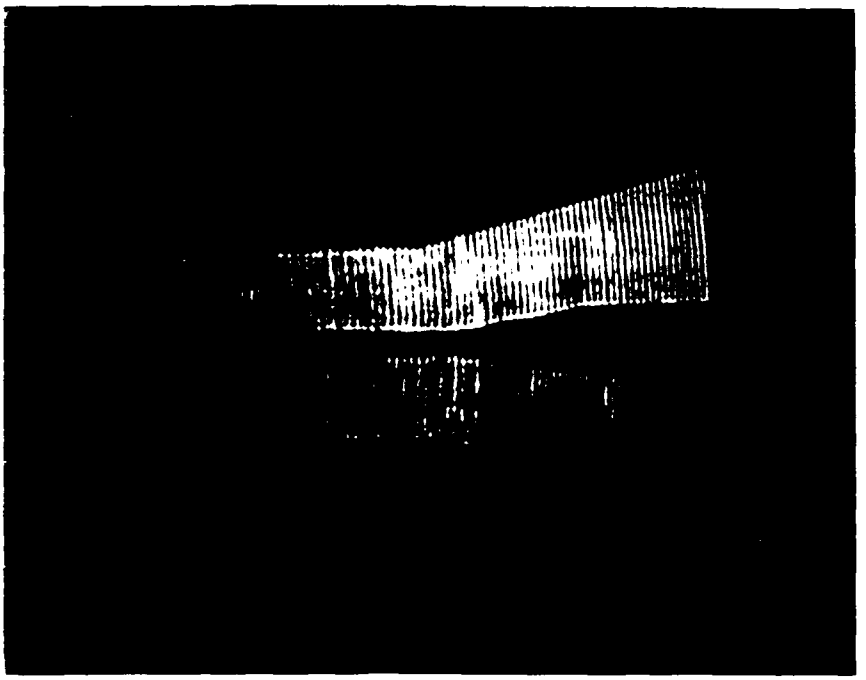

Figure 2 Reconstructed hologram of a wedge-shaped object before flow. The fine line structure is due to multiple reflections between the crystal surfaces.

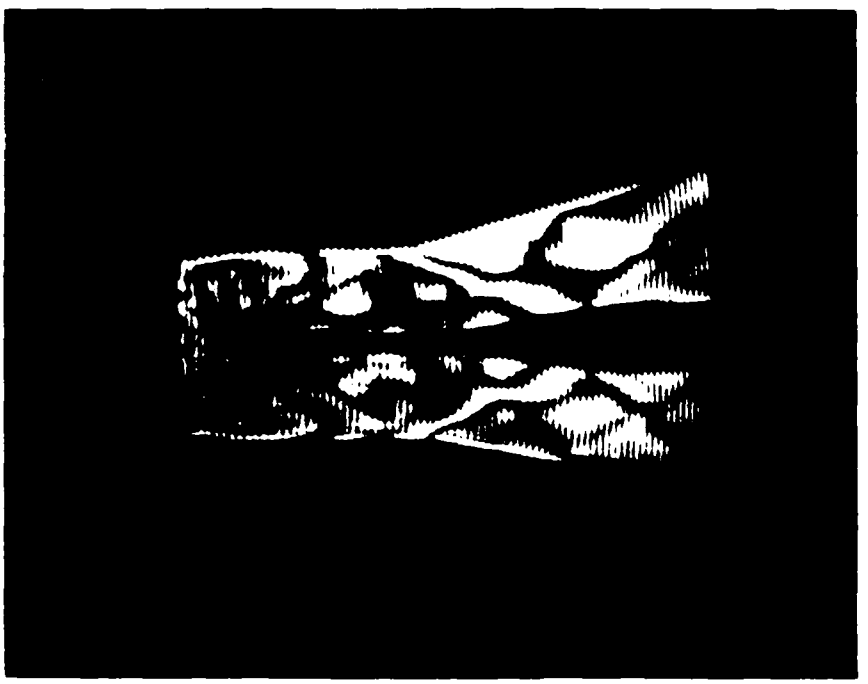

Figure 3 Output interferogram produced by double-exposure holography. The second exposure is made on top of the hologram in Fig.2 but with the flow on.

index constitutes the stored hologram grating. This basic effect is now called the photorefractive effect.[6]

EXPERIMENTS

In this paper, experimental production of interferograms using a high-power argon laser and double-exposure holography in lithium niobate crystals is reported. The system shown in Fig. 1 has been used to visualize flow-field patterns in a wind tunnel for a variety of different test objects. A high-power cw Argon-ion laser with a single-frequency line of 514.5 nm wavelength is used. The beam splitter divides the beam into an object beam and a reference beam. The object beam is collimated to a diameter of 50 mm. It passes through the wind tunnel window and then through a Fourier transform lens. The reference beam is slightly focused to a desired diameter using a long focal-length converging lens to achieve optimum overlap of the two beams. A polarization rotator is placed in the reference beam to control the readout polarization of the stored holograms (s or p polarization readout). The two beams meet at a point 5 mm away from the focal plane of the Fourier transformed object wave. The external Bragg angle at that point is 15°. The 0.05% iron-doped lithium niobate crystal is used in the transmission geometry configuration. The two beams are s-polarized when recording the holograms. The crystal allows recording in various locations because its dimensions are significantly larger (10 mm X 10 mm X 1.6 mm) than the small size spot areas that are used for the holograms. The object beam has a cross-sectional area of approximately 1 mm^2 (at the crystal) while the reference beam is approximately 3 mm^2 to make certain that full overlap is obtained. Typically, the power density used in these experiments is 16 W/cm^2 for the two beams combined. Reference (R) to object (S) beam ratio is on the order of 3 ($R/S \cong 3$).

As an example, Fig. 2 shows a reconstructed single-exposure hologram of one of these objects with the corresponding double-exposure flow visualization shown on the interferogram in Fig. 3. The result in Fig. 3 was obtained using two 30 msec exposures with the resulting output interferogram immediately available without a separate development step or removal of the crystal from the system.

CONCLUSIONS

Holographic interferometry using photorefractive crystals has been reported. Lithium niobate is a well-suited material for this application. Simultaneous recording and storage of double exposure holograms can be achieved via angular multiplexing. Angular packing density of several (double-exposure) holograms per degree can be used without appreciable crosstalk. The technique used is highly sensitive. Changes in the aerodynamic conditions (pressure and object physical shape) produce clearly observable differences in the results.

ACKNOWLEDGMENT

This work was supported by the U.S. Army Research Office under grant number DAAL03-86-K-0149.

REFERENCES

1. R. Magnusson, J. H. Mitchell III, T. D. Black, and D. R. Wilson, "Holographic Interferometry Using Iron-Doped Lithium Niobate", Appl. Phys. Lett. 51, 81 (1987).

2. J. P. Huignard, and J. P. Herriau, "Real-Time Double-Exposure Interferometry with $Bi_{12}SiO_{20}$ Crystals in Transverse Electrooptic Configuration", Appl. Opt. 16, 1807 (1977).

3. A. Marrakchi, J. P. Herriau, and J. P. Huignard, "Real-Time Holographic Interferometry with Photorefractive $Bi_{12}SiO_{20}$ Crystals", Proc. S.P.I.E. 353, 24 (1982).

4. J. P. Huignard, J. P. Herriau, and T. Valentin, "Time Average Holographic Interferometry with Photoconductive Electrooptic $Bi_{12}SiO_{20}$ Crystals". Appl. Opt. 16, 2796 (1977).

5. Y. H. Ja, "Real-Time Double-Exposure Holographic Interferometry in Four-Wave Mixing With Photorefractive $Bi_{12}GeO_{20}$ Crystals", Appl. Opt. 21, 3230 (1982).

6. A. M. Glass, "The Photorefractive Effect", Opt. Eng. 17, 470 (1978).

Holographic interferometry using iron-doped lithium niobate

R. Magnusson and J. H. Mitchell, III
Department of Electrical Engineering, The University of Texas at Arlington, Arlington, Texas 76019

T. D. Black
Department of Physics, The University of Texas at Arlington, Arlington, Texas 76019

D. R. Wilson
Department of Aerospace Engineering, The University of Texas at Arlington, Arlington, Texas 76019

(Received 30 December 1986; accepted for publication 14 May 1987)

Holographic interferometry using crystals of iron-doped lithium niobate is reported. The interferograms presented are produced via double-exposure Fourier transform holography in heavily doped crystals without applied electric fields. Flow-field visualization is used as an example application area.

Photorefractive crystals such as lithium niobate ($LiNbO_3$) possess properties that make them well suited for holographic interferometry applications. These properties include instantaneous hologram formation (self-development), high data storage capacity via volume superposition, high sensitivity and resolution, erasability and reusability, fast recording and readout, and hologram fixing.[1] It is predicted that these and other features will make photorefractive media increasingly important for interferometry. To date, however, very little research has been conducted for defining in detail the applicability of this class of materials for interferometry.

The basic process of hologram formation in $LiNbO_3$ can be described generally as follows: With the crystal placed at the intersection of two (interfering) laser beams, electrons are excited from traps within the bright fringes of the interference pattern. These electrons then migrate out of the bright fringes and are retrapped in the dark fringes. The resulting spatially varying charge distribution creates space-charge fields that modulate the refractive index of the crystal via the electro-optic effect. This spatially varying refractive index constitutes the stored hologram grating.

Holographic interferometry using the photorefractive effect has previously been demonstrated using bismuth silicon oxide (BSO) and bismuth germanium oxide (BGO) crystals. Huignard and Herriau[2] produced real-time double-exposure interferograms with BSO crystals. These crystals are very sensitive at argon-ion laser wavelengths requiring similar energy densities as silver halide photographic emulsions but also requiring the application of an external electric field. Furthermore, due to this high sensitivity, retention time is very short and readout is destructive. Huignard *et al.* also presented results on time-average holographic interferometry using this material.[3] Real-time interferometry in four-wave mixing using bismuth germanium oxide (BGO) crystals has been demonstrated by Ja.[4] In this experiment, a reflection-type geometry was used without an external electric field yielding interferograms with a short lifetime (~ 1 s).

In this letter, production of interferograms via double-exposure holography in crystals of lithium niobate without an applied electric field is reported. Interferograms of good quality of a variety of amplitude and phase objects have been produced with these crystals in both reflection geometry and transmission geometry. Special emphasis is placed on visualization of flowfield features for aerodynamic applications as this area stands to benefit greatly by the development of improved materials and procedures for interferometry.

Figure 1 illustrates the system used to produce the results presented (transmission geometry only). The argon-ion laser beam, operating at $\lambda = 514.5$ nm, is split into two beams by the beam splitter. The reference beam is used directly whereas the object beam is spatially filtered, expanded, and collimated. The collimated beam, now with a diameter of 3 cm, propagates through the test chamber of the wind tunnel to a Fourier transforming lens ($f = 30$ cm) that reduces the object beam down to a small area in the crystal, which is located between 1 and 2 cm in front of the back focal plane of the lens. The spot size of each beam at the plane of the crystal is approximately 5 mm^2 because of the slightly

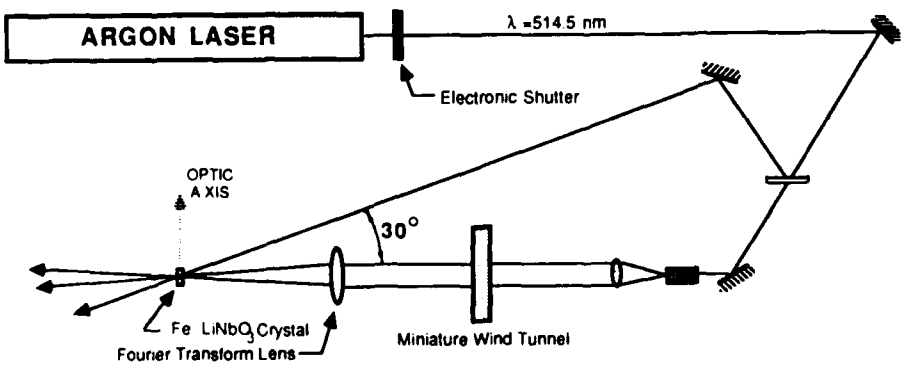

FIG. 1. Experimental system.

 0003-6951/87/280081-02$01.00

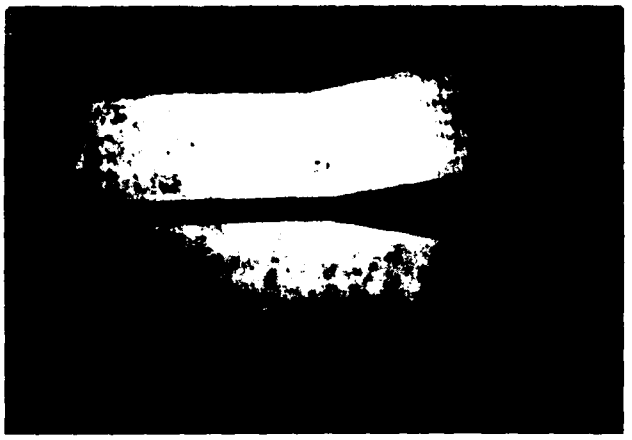

FIG. 2. Reconstructed hologram of object area without flow to demonstrate inherent optical system noise.

FIG. 3. Reconstructed hologram of transonic flow field showing shock wave structure around airfoil.

out-of-focus Fourier transform geometry used. The two laser beams intersect at an angle of 30° and are polarized perpendicular to the plane of incidence at the crystal.

The crystal (10 mm × 10 mm × 1.4 mm) used in these experiments is heavily doped with iron or at a level of 0.1 mole % Fe. The absorption coefficient was found to be 22 cm^{-1}. The orientation of the crystal is critical. For maximum sensitivity, the holographic interference fringes must be orthogonal to the crystal optical axis to take advantage of the built-in photovoltaic effect[1] of $LiNbO_3$ for the charge transport. The optical quality of the crystal used is quite good as illustrated in Fig. 2. This figure is a photograph of a reconstructed double-exposure hologram that was recorded without flow for the purpose of demonstrating the inherent low noise of the optical system. Double-exposure is used in Fig. 2 for consistency and to illustrate system stability. Figure 3 was recorded under identical conditions except that the second holographic exposure was made at full-flow pressure. Thus, both a no-flow reference hologram and a full-flow hologram are recorded in the crystal. Upon reconstruction, the object waves corresponding to the holograms of these two flow states interfere, revealing the shock waves present during flow. The reference (no-flow) exposure is, thus, necessary to produce the output fringe structure by which the flow is visualized. The results shown in Fig. 3 were produced with a beam ratio (reference-beam to object-beam power) of 2.35 and 480 mW of cw total laser beam power with 1 s exposures. The diffraction efficiency was approximately 1%.

Preliminary experiments with volume superposition of double-exposure holograms in this material are promising. Several such holograms have been angularly multiplexed with 0.5° crystal rotation between exposures. The interferograms produced upon reconstruction were of good quality and exhibited only small degrees of crosstalk.

In conclusion, holographic interferometry using crystals of iron-doped lithium niobate has been reported. Interferograms of high quality can be obtained. The results are immediately available (no development needed) and the interferometer can be operated under normal illumination (a darkened work area is not required). Whereas BSO and BGO appear to be most useful in real-time or near-real-time applications, lithium niobate possesses the additional feature of possible simultaneous recording and storage of double-exposure holograms via Bragg angular multiplexing. These materials will find increasing use in experimental aerodynamics and other application areas of interferometry.

The authors thank T.L. Estle and S.F. Su for supplying the crystals used and D.A. Larson for sample preparation. This work was supported by the U.S. Army Research Office under grant number DAAL03-86-K-0149.

[1] A. M. Glass, Opt. Eng. **17**, 470 (1978).
[2] J. P. Huignard and J. P. Herriau, Appl. Opt. **16**, 1807 (1977).
[3] J. P. Huignard, J. P. Herriau, and F. Valentin, Appl. Opt. **16**, 2796 (1977).
[4] Y. H. Ja, Appl. Opt. **21**, 3230 (1982).

Reprinted from Applied Optics

Visualization of aerodynamic flow fields using photorefractive crystals

A. Hafiz, R. Magnusson, J. S. Bagby, D. R. Wilson, and T. D. Black

Interferometry based on double exposure Fourier transform holography in photorefractive crystals is applied for visualization of aerodynamic flow fields. The interferograms obtained are of similar quality as those produced using holographic film but with greatly simplified procedures. The results presented are obtained using a high-power cw argon laser and iron doped lithium niobate crystals. The angular characteristics of the Fourier transform data holograms are studied.

I. Introduction

Holographic interferometry is an important diagnostic technique with a large number of practical applications. Global visualization of spatial refractive index distributions may be obtained using this technique. Example application areas include aerodynamics, plasma diagnostics, and heat transfer. Holographic interferometry allows the resultant refractive index distributions to be quantitatively evaluated in these cases without disturbing the flow.

To date, holographic film has been used as the recording medium in most of the holographic interferometry experiments reported in the literature. The use of film is basically undesirable due to the tedium involved in developing the exposed film and due to the necessity of a darkened work area. Self-developing or photorefractive optical crystals offer an alternative to the use of film in holographic interferometry. In this paper, interferometric visualization of aerodynamic flow fields using photorefractive crystals is reported.

Photorefractive crystals have many favorable characteristics for holographic interferometry. These include instantaneous hologram storage (no development needed), large information storage capacity via angular multiplexing, erasability and reusability, available hologram fixing techniques, wide hologram lifetime range, real time recording and readout, high sensitivity and resolution, controllable materials properties, and, at last, sensitivity to laser recording light only with no need to work in the dark. Hologram recording in such materials is based on the photorefractive effect.[1]

Only limited amount of research has been done on interferometry using photorefractive crystals as the storage medium. Magnusson *et al.*[2] reported initial experimental results in iron doped lithium niobate where a relatively low power laser was used requiring long exposures (~1 s). Real time, double exposure interferograms have been produced with bismuth silicon oxide (BSO) crystals.[3,4] These crystals are very sensitive at argon-ion laser wavelengths (in the blue and the green spectral region), requiring similar energy densities as silver halide photographic emulsions but also requiring the application of an external electric field. Due to this high sensitivity, retention time is very short and readout is destructive. Thus, while reading, the interferometric image should be stored, for example, via a vidicon tube for further processing. These workers have also presented results on time average holographic interferometry using this material.[5] Real time interferometry in four-wave mixing using bismuth germanium oxide (BGO) crystals has also been demonstrated.[6] In that experiment, a reflection type geometry was used without an external electric field yielding interferograms with a short lifetime (~1 s). BSO and BGO thus appear to be most useful in real time or near real time applications while volume hologram superpositions are not feasible in these crystals due to their high sensitivity.

This paper presents experimental work on aerodynamic flow field visualization using double exposure hologram recording in lithium niobate crystals doped with iron ($Fe:LiNbO_3$). In the current experiments, many objects are used and holograms produced with exposure times around 10–50 ms are presented. The

All authors are with University of Texas at Arlington, Arlington, Texas 76019; D. R. Wilson is in the Department of Aerospace Engineering, T. D. Black is in the Department of Physics, and the other authors are in the Department of Electrical Engineering.

Received 22 June 1988.
0003-6935/89/081521-04$02.00/0.

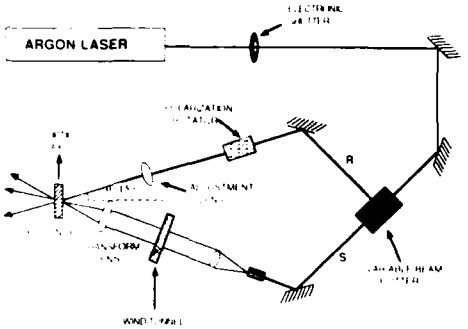

Fig. 1. Experimental system.

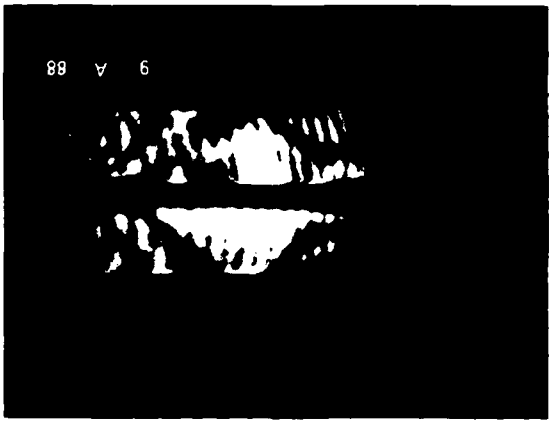

Fig. 2. Interferogram of the flow field in the wind tunnel. The object is circularly symmetric with a ball tip. The pressure is 220 psi.

results are greatly improved over those previously reported.[2] The different objects used in this work demonstrate the sensitivity of the flow to the target physical shape and the ability of the technique used to record these differences. It is also demonstrated that good sensitivity to varying flow conditions for a given object is obtained. Multiple storage of interferograms via angular multiplexing is demonstrated.

II. Experiments

The experimental system is shown in Fig. 1. A high power cw argon-ion laser with a single frequency line of 514.5-nm wavelength is used. The beam splitter divides the beam into an object beam and a reference beam. The object beam is collimated to a diameter of 50 mm. It passes through the wind tunnel window and then through a Fourier transform lens. The reference beam is slightly focused to a desired diameter using a long focal length converging lens to achieve optimum overlap of the two beams. A polarization rotator is placed in the reference beam to control the readout polarization of the stored holograms (s- or p-polarization readout). The two beams meet at a point 5 mm away from the focal plane of the Fourier transformed object wave. The external Bragg angle at that point is 15°. The 0.05% iron doped lithium niobate crystal is used in the transmission geometry configuration. It is of vital importance that the crystal optic axis is oriented orthogonal to the holographic fringes to take advantage of the photovoltaic effect and the attendant efficient charge transport. The two beams are s-polarized when recording the holograms. The crystal allows recording in various locations because its dimensions are significantly larger (10 × 10 × 1.6 mm) than the small size spot areas that are used for the holograms. The object beam has a cross sectional area of ~1 mm^2 (at the crystal) while the reference beam is ~3 mm^2 to make certain that full overlap is obtained. Typically, the power density used in these experiments is ~16 W/cm^2 for the two beams combined. Reference (R) to object (S) beam ratio is of the order of 3 (R/S ≅ 3).

The wind tunnel is driven by nitrogen gas and the flow fields for the objects of different sizes and shapes are recorded. The first interferogram is recorded under symmetric conditions (unslanted holograms) whereas the rest are written via angular multiplexing with ~0.1–1° angular spacing (achieved by crystal rotation) between the double exposure holograms. The experiment is performed in many different configurations. The holographic exposure is set to various values, typically 10–50 ms.

III. Results

The object mounted in the wind tunnel for the experiments reported here is circularly symmetric with a ball tip. The object wave thus traverses what is actually a 3-D flow structure. If the objects were constant along the laser beam direction (i.e., spanned across the wind tunnel), improved fringe contrast would be obtained. The wind tunnel window has dimensions of 10 × 20 mm.

An interferogram produced by the reconstruction of a double exposure hologram (first exposure, flow off; second exposure, flow on) is shown in Fig. 2. This demonstrates the visualization of the flow field created by this object. The shock waves generated by the object and bouncing off the tunnel walls are clearly shown. The input pressure used is 220 psi. Two 30-ms exposures are used. The total laser power is 16 W/cm^2. The superimposed fine line structure is due to multiple internal reflections between the crystal surfaces.

To demonstrate the sensitivity of this technique to variations in the aerodynamic conditions, additional visualizations are produced under varying flow pressure. Figure 3 is similar to Fig. 2 except that the input flow pressure is now 270 psi, with corresponding increased fringe density and higher bow-wave angle. Figure 4 is similar but at 320 psi. Note the shock waves bouncing off the tunnel walls.

A variety of test objects have been used during the course of this work under widely varying experimental conditions. The experimental results are easily and conveniently obtained. Sequential recording is accomplished using angular multiplexing of the double exposure holograms. For the data in Figs. 2–4, the interferograms are angularly multiplexed with the (external) angular separation $\Delta\theta' = 0.5°$. Each double exposure hologram is reconstructed on the Bragg angle. In Fig. 5 an example interferogram produced via

Fig. 3. Similar to Fig. 2 but with 270-psi pressure.

Fig. 4. Similar to Fig. 2 but at 320 psi.

angularly stacked holograms (in the same physical crystal location) is shown. The same object is used. This interferogram corresponds to the thirteenth in a set of double exposure holograms, all recrecorded under different conditions and with several different objects. Note that the quality of the interferogram has not substantially deteriorated over that of Figs. 2–4.

To further quantify the storage of multiple double exposure holograms via angular multiplexing, several sets of interferograms have been produced with the diffraction efficiency and angular selectivity of each such hologram measured. A curve of the diffraction efficiency vs the readout angle is presented in Fig. 6. In this collection of holograms, the change in the Bragg angle was $\Delta\theta' = 1.0°$. All the interferograms were recorded under the same conditions with two 30-ms exposures used for each. Typical diffraction efficiency for s-polarization readout is seen in this figure to be 0.7–1.0%. The sidelobe structure is sketched using the analytical expression for diffraction efficiency from the Kogelnik theory,[7] matching the theory and the experiment on the Bragg angle only. The diffraction efficiency is given by

$$\eta = \sin^2[(\gamma^2 + \xi^2)^{1/2}]/(1 + \xi^2/\gamma^2), \quad (1)$$

where $\gamma = \pi n_1 d/[\lambda(c_R c_S)^{1/2}]$ is the modulation coefficient, $\xi = \upsilon d/(2c_S)$, n_1 is the amplitude of the sinusoidal

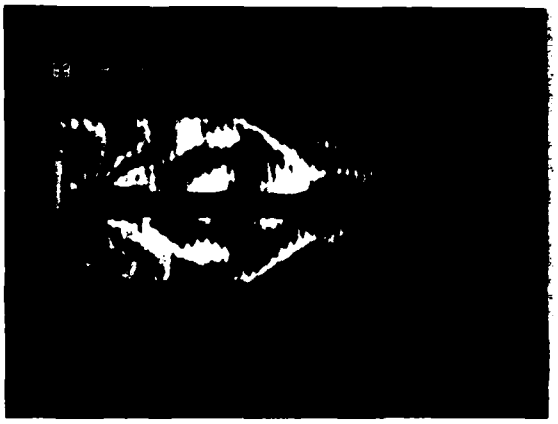

Fig. 5. Interferogram corresponding to the thirteenth angularly multiplexed double exposure hologram in a stack storing a sequence of flow field visualization results. The object is the same as that in Fig. 2, and the angular separation is $\Delta\theta' = 0.5°$.

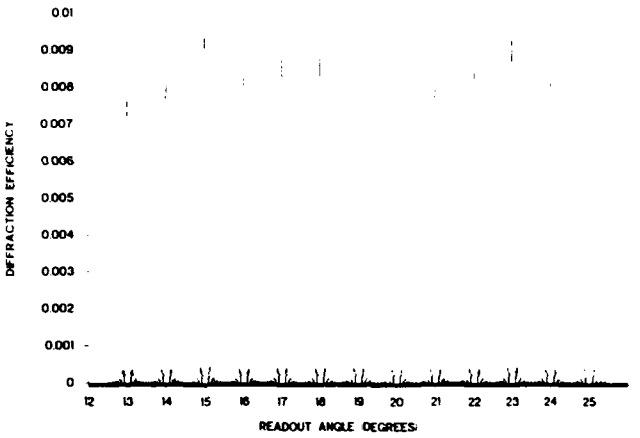

Fig. 6. Angularly multiplexed double exposure holograms. The diffraction efficiency vs the (external) readout angle is shown. The crystal thickness is 1.6 mm.

index modulation, d is the thickness of the crystal, λ is the free-space wavelength, $c_R = \cos\theta$ and $c_S = \cos\theta - \lambda \cos\phi/(n_0\Lambda)$ are the obliquity factors, υ is the dephasing measure given by $\upsilon = \pi[2\cos(\phi - \theta) - \lambda/(n_0\Lambda)]/\Lambda$, n_0 is the bulk index of refraction, Λ is the grating spacing, ϕ is the slant angle, and θ is the internal readout angle. This is done to give an indication of the angular spread of the holograms in practice. In Fig. 7, it is indeed verified that the theory gives a reasonable estimate of the angular behavior. There, the angular selectivity of a single double exposure hologram with a Bragg angle of $\theta' = 15°$ is examined more carefully. Theory as represented by Eq. (1) and experiment are compared, matching the two at the Bragg angle. The theory intended to describe infinite plane wave readout of thick hologram gratings is seen to describe adequately the much more complicated situation of two superimposed Fourier transform data holograms, at least for the experimental conditions used here.

IV. Conclusions

Holographic interferometry using photorefractive crystals has been reported. Lithium niobate crystals

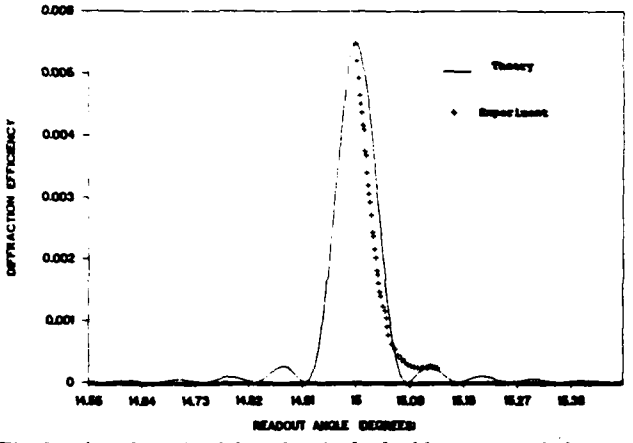

Fig. 7. Angular selectivity of a single double exposure hologram recorded in the crystal used in Fig. 6.

are well suited for this application. Simultaneous recording and storage of double exposure holograms is demonstrated via angular multiplexing. Angular packing density of more than two (double exposure) holograms per degree can be used with no crosstalk observed. The sensitivity of the technique used is also demonstrated. Changes in the aerodynamic conditions (pressure and object physical shape) produce clearly observable differences in the results. The resolution provided by the crystals is, therefore, ample for applications in aerodynamic flow field visualization.

This work was supported by the U.S. Army Research Office under grant DAA L03-86-K0149. The assistance of D. Shin in the laboratory is acknowledged.

References

1. A. M. Glass, "Photorefractive Effect," Opt. Eng. 17, 470 (1978).
2. R. Magnusson, J. H. Mitchell III, T. D. Black, and D. R. Wilson, "Holographic Interferometry Using Iron-Doped Lithium Niobate," Appl. Phys. Lett. 51, 81 (1987).
3. J. P. Huignard, and J. P. Herriau, "Real-Time Double-Exposure Interferometry with $Bi_{12}SiO_{20}$ Crystals in Transverse Electrooptic Configuration," Appl. Opt. 16, 1807 (1977).
4. A. Marrakchi, J. P. Herriau, and J. P. Huignard, "Real-Time Holographic Interferometry with Photorefractive $Bi_{12}SiO_{20}$ Crystals," Proc. Soc. Photo-Opt. Instrum. Eng. 353, 24 (1982).
5. J. P. Huignard, J. P. Herriau, and T. Valentin, "Time Average Holographic Interferometry with Photoconductive Electrooptic $Bi_{12}SiO_{20}$ Crystals," Appl. Opt. 16, 2796 (1977).
6. Y. H. Ja, "Real-Time Double-Exposure Holographic Interferometry in Four-Wave Mixing with Photorefractive $Bi_{12}GeO_{20}$ Crystals," Appl. Opt. 21, 3230 (1982).
7. H. Kogelnik, "Coupled Wave Theory for Thick Hologram Gratings," Bell Syst. Tech. J. 48, 2909 (1969).

R. Magnusson

A. Hafiz

J. S. Bagby

Department of Electrical Engineering.

A. Haji-Sheikh

Department of Mechanical Engineering.

The University of Texas at Arlington, Arlington, Texas 76019

Holographic Interferometry Using Self-Developing Optical Crystals for Heat Flux Evaluation

Double-exposure holographic interferometry with crystals of iron-doped lithium niobate as the storage material is applied to study heat transfer from electronic chips. These crystals are self-developing, making the reults immediately available for use. This method of interferometry can be used to study the temperature field in heating and cooling fluids. In particular, it is a practical method for studying the heat transfer from small devices such as microelectronic chips. Double-exposure holographic interferometry is a viable experimental technique in transient as well as steady-state problems.

Introduction

The use of holographic interferometry for a wide variety of practical applications is now well established. During the past few years, this basic technique and its numerous variants have been developed and applied in many different situations (Vest, 1979; Hariharan, 1984). In particular, this technique is extremely well suited for experiment heat transfer, aerodynamics, and plasma diagnostics. Holographic interferometry yields global spatial visualization of refractive-index distributions with quantitative results without affecting the phenomena under study.

The recording medium in most of the holographic interferometry experiments reported to date has been film, yielding good results when relatively few exposures (frames) are to be recorded or a steady-state phenomenon is under study. In time-varying flow visualization experiments, the use of film may be more difficult due to the large number and speed of needed exposures, mechanical film movement, the tedium of development, and other problems. Therefore, for the following reasons, photorefractive, or electro-optic, media may be the optimum recording media for these applications:

1) Holograms are stored virtually instantaneously by charge migration and the electro-optic effect (Glass, 1978). Thus no development is needed.

2) Huge information storage capacity (theoretically 10^{12} bits/cm^3) via angular multiplexing.

3) Erasable and reusable without fatigue.

4) Holograms can be fixed (i.e., infinite retention of stored data).

5) Wide range of hologram lifetime: From years or months to less than a microsecond.

6) Real-time recording and readout is possible.

7) High sensitivity and resolution.

8) Controllable material properties. Media and properties can be selected to suit a particular application.

9) Only sensitive to the recording light. Thus, it is not necessary to work in total darkness.

Little research has been done on interferometry using photorefractive crystals as the storage medium. Real-time double-exposure interferograms have been produced with bismuth silicon oxide (BSO) crystals (Huignard and Herriau, 1977, and Marrakchi et al., 1982). These crystals are very sensitive in the blue and the green spectral regions, requiring energy densities similar to silver halide photographic emulsions but also requiring the application of an external electric field. Retention time is, therefore, very short and readout is destructive. Huignard and coworkers have presented results on time-average holographic interferometry using this material (Huignard et al., 1977). Real-time interferometry in four-wave mixing using bismuth germanium oxide (BGO) crystals has also been demonstrated (Ja, 1982). In that experiment, a reflection-type geometry was used without an external electric field, yielding interferograms with a short lifetime ($\sim$ 1 s). Magnusson et al. (1987) reported initial experimental results in iron-doped lithium niobate using a low-power laser, thus requiring rather long exposures ($\sim$ 1 s). BSO and BGO appears to be most useful in real-time or near-real-time applications while volume hologram superpositions are not feasible in these crystals due to rapid decay of the holograms.

The purpose of this paper is to present experimental results on visualization of thermally-induced refractive-index spatial distributions using double-exposure hologram recording in lithium niobate crystals doped with iron (Fe:$LiNbO_3$). The techniques presented are useful in experimental heat-transfer studies. The example objects used are electronic chips in air and in water. The holograms are produced with exposure times around 50–100 ms. Fourier-transform holography allows multiple storage of interferograms via angular multiplexing in these relatively small ($10 \times 10 \times 2$ mm^3) crystals. The holograms form vitually instantaneously since the charge migration processes are extremely fast. Therefore,

Contributed by the Electrical and Electronics Packaging Division for publication in the JOURNAL OF ELECTRONIC PACKAGING. Manuscript received by the Electrical and Electronics Packaging Division May 22, 1989; revised manuscript received May 10, 1990.

these media are self-developing. No processing or removal of the medium from the recording system is required. In addition, these media are reusable, erasable, and exhibit no fatigue. Erasure is possible optically or thermally by heating the crystal to 200°C.

Photorefractive Crystals

Optically induced changes of the refractive index of electro-optic crystals were first reported by Ashkin et al. (1966). Initially, this effect was referred to as optical, or laser, damage, as it was detrimental to the intended applications. Subsequently, it was realized that such an effect could be useful in applications requiring that optically-induced spatial patterns (such as gratings) be formed directly upon exposure (i.e., self-development). Holographic storage in lithium niobate ($LiNbO_3$) was reported in 1968 by Chen et al. This effect is now called the *photorefractive effect* in analogy with the photochromic effect (optically-induced changes in absorption).

The basic process of hologram formation in a photorefractive medium can be described generally as follows: With the crystal placed at the intersection of two (interfering) laser beams, electrons are excited from traps within the bright fringes of the interference pattern. These electrons then migrate out of the bright fringes and are retrapped in the dark fringes. The resulting spatially-varying charge distribution creates space-charge fields that modulate the refractive index of the crystal via the electro-optic effect. This spatially varying refractive index constitutes the stored hologram grating.

The photorefractive effect has been observed in numerous media. These include lithium niobate and lithium tantalate (Ashkin et al., 1966 and Chen et al., 1968), bismuth silicon oxide (BSO) and bismuth germanium oxide (BGO) (Huignard and Micheron, 1976) strontium barium niobate (Thaxter, 1969), barium titanate (Feinberg et al., 1980), potassium tantalum niobate (KTN) (Chen, 1967), and, more recently, gallium arsenide and indium phosphide (Glass et al., 1984). Although these materials all have the photorefractive effect in common, the detailed processes of charge excitation, charge migration, and retrapping vary significantly from one material to the next. In $LiNbO_3$, the photorefractive sensitivity is greatly enhanced by doping the crystal with iron. The amount of iron doping and the valence state of the iron atoms within the host material are important factors in this respect. The photocarrier excitation mechanism of the photorefractive effect in iron-doped lithium niobate can consequently be described by the reaction (Glass, 1978):

$$Fe^{2+} + h\nu = Fe^{3+} + \text{free electron} \qquad (1)$$

where $h\nu$ represents the energy of the absorbed light photon. Also, the Fe^{3+} ions function as the electron traps; therefore, the net result of the exposure of the crystal to the light interference pattern is a spatial variation of the Fe^{2+}/Fe^{3+} ratio.

Experiments

The holographic interferometer is shown in Fig 1. The

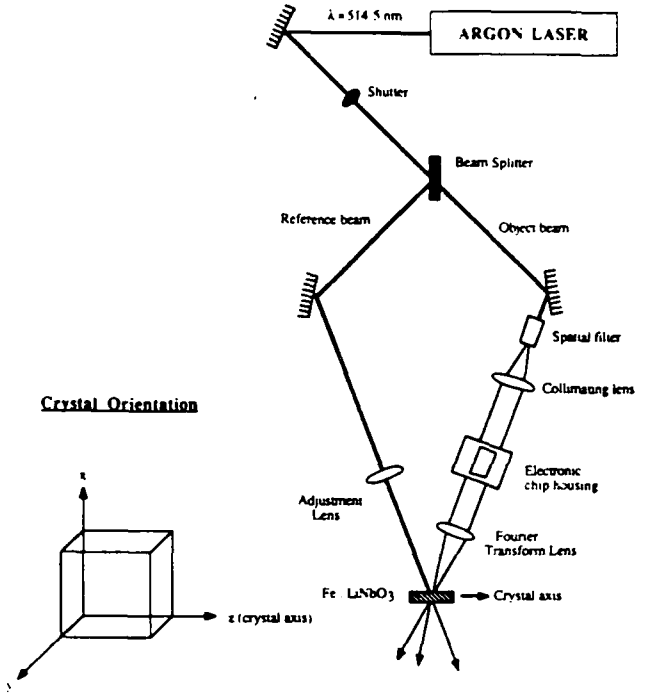

Fig. 1 Experimental system

variable beam splitter divides the beam of a high power continuous-wave argon-ion laser ($\lambda = 514.5$ nm) into two waves. The object beam travels through a spatial filter (a lens and a pinhole) and is then collimated by a separate lens into a plane wave with a diameter of 50 mm. The object (an electronic chip) is placed at a distance 30 cm in front of the Fourier transform lens. The reference beam passes through a focusing lens to adjust the spot area and to control the input power density. The reference and object beams intersect in the crystal that is located 10 mm away from the back focal plane of the Fourier transform lens. This out-of-focus approach is used to avoid saturation of the material due to the high power densities exactly in the focal plane. The angle between the reference beam and the object beam is 30 deg. The crystal transverse dimensions 10×10 mm^2 permit recording at various locations in the crystal volume because of the small spot areas of the two beams. This implies high data storage capacity when employing the angular multiplexing technique. In the current experiments, the reference and object beams have 3.8 and 2.8 mm^2 spot areas, respectively. The 0.05 percent iron-doped lithium niobate crystal used in this experiment is *y*-cut.

The IC chip used is a commercial isolated resistor network, Allen-Bradley type 316B220. It is a dual-in-line package with a solid ceramic body containing 8 resistors 22 ohms each. The electronic chip is heated by applying a voltage to it. Initially, one resistor was calibrated to serve as a resistance thermometer. However, at a higher range of temperatures, the thermally-induced carriers cause the resistance to change and correlation becomes unpredictable due to the complexity of

Nomenclature

A = area, m^2
Bi = $h(V/A)/k$ = Biot number
g = gravitational acceleration, m/s^2
$\bar{h}$ = average heat transfer coefficient, W/m^2-K
h = heat transfer coefficient, W/m^2-K
H = height, m
I = intensity of radiation, W/m^2
k = thermal conductivity, W/m-K
L = length, m
L_c = $HL/(H+L)$ = characteristic length, m
n = length along the outer normal
Nu = hL_c/k = Nusselt number
q = power dissipated, W
Ra = $g\beta(T_c - T_a)L_c^3/\nu\alpha$ = Rayleigh number
T_a = ambient temperature, °C
T_c = chip temperature, °C
V = volume, m^3
α = thermal diffusivity, m^2/s
β = thermal expansion coefficient, K^{-1}
ν = kinematic viscosity, m^2/s

the internal geometry. It is assumed that the resulting temperature distribution in the chip is uniform. This assumption is valid if the ratio of the internal (or conductive) resistance to the external (or convective) thermal resistance is negligible. This concept is often quantified by defining a dimensionless quantity called the Biot number, $Bi = h(V_{chip}/A_{chip})/k_{chip}$, and requiring that $Bi < 0.1$. In this study, the Biot number is generally less than 0.01. For these reasons, the temperature is monitored by attaching a thermocouple to the bottom surface of the chip. The chip dimensions are $21.5 \times 6.4 \times 2$ mm^3. The reference (R) to object (S) beam ratio is approximately R/S = 4. The explosure levels are typically 50–100 ms for each hologram at around 30W/cm^2 laser power density. The reading power density is typically 60mW/cm^2. The room temperature was 25.6°C. The two beams are *s* polarized; that is, the electric field of the optical beam is perpendicular to the plane of incidence. The system is mounted on a rigid, vibration isolation table. Crystal rotation is achieved using a programmable motion control system.

The experimental diffraction efficiency, DE, of a hologram is defined as

$$DE = I_d/(I_o - I_r) \qquad (2)$$

where I_d is the diffracted intensity, I_o is the input intensity, and I_r is the reflected intensity. This quantity, thus, indicates the power in the beam diffracted by the hologram and containing the information of interest. Efficiency of 1 percent or lower is usually sufficient to get good reconstruction and interferograms.

Results

The holographic interferometer shown in Fig. 1 is used to obtain the results reported in this paper. The procedure for recording a double-exposure hologram is straightforward. The first step is to record a hologram of the chip with zero voltage (voltage off) applied. Then another hologram is superimposed on the previous one with the required voltage (voltage on) applied. Retrieving the information is achieved by blocking the object beam and reading the data (i.e., double-exposure hologram reconstruction) with the reference beam. This reconstructed wave will travel in the direction of the original object waves. The interference of the two simultaneously reconstructed object waves produces the interferogram that can be viewed on a screen.

The first set of interferograms is shown in Fig. 2. Five double-exposure holograms were recorded with precise angular positions obtained with the programmable motion control system. The voltage-off scenes were sequentially written at angles with $\Delta\theta = 0.5$ deg separation. These same angular locations were then recalled by the programmable system and the corresponding voltage-on holograms recorded. In Fig. 2, the first, third, and fifth of the corresponding output interferograms are shown. The density of fringes is seen to increase with the temperature of the chip. The lack of symmetry in the figures is caused by a slight plume oscillation and imperfection of the geometry. These oscillations (and other transients in these experiments) were much slower than the 5—100 ms exposure times used and thus did not affect the photographic images. The small spacing between fringes along the side and near the edges are indicative of high heat flux. Away from the chip, the widening of the spacing between the dark lines indicates smaller temperature gradients. The vertical fine line structure is due to multiple internal reflections between the optically flat and polished crystal faces. It is more convenient to use this sequential approach rather than heating and cooling the chip each time (at a fixed angular position) to obtain the required double-exposure hologram for the two states. In the same $(x - z)$ crystal location, 20 double-exposure holograms were angularly multiplexed without significant degradation or noise buildup. The diffraction efficiency varied between 1-3 percent.

Fig. 2(a)

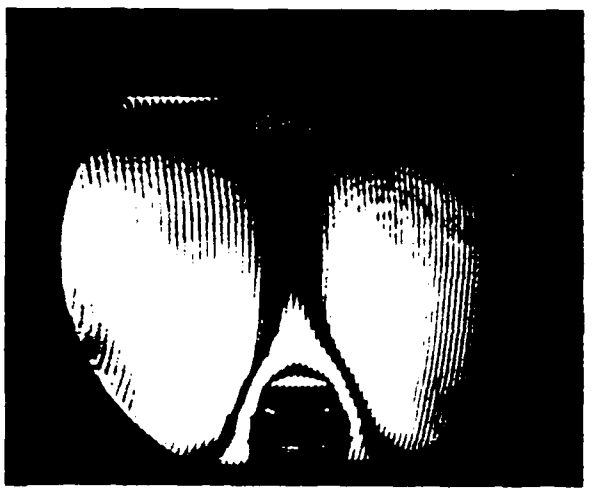

Fig. 2(b)

Fig. 2(c)

Fig. 2 Fringe structure development as a result of heat transfer from a heated IC chip. The aluminum plate is 4 cm from the chip top surface. (a) $q = 0.57$W, $T_c = 56.9$°C (b) $q = 1.11$W, $T_c = 84.6$°C (c) $q = 3.55$W, $T_c = 139.9$°C.

Figure 3 shows two interferograms of orthogonal views through the heat transfer volume. The temperature of the chip surface is 226°C as measured by the thermocouple. An arbitrary number of different views can be taken for such experiments. The ideal approach is to mount the object also on a computer-controlled rotational stage and then proceed as

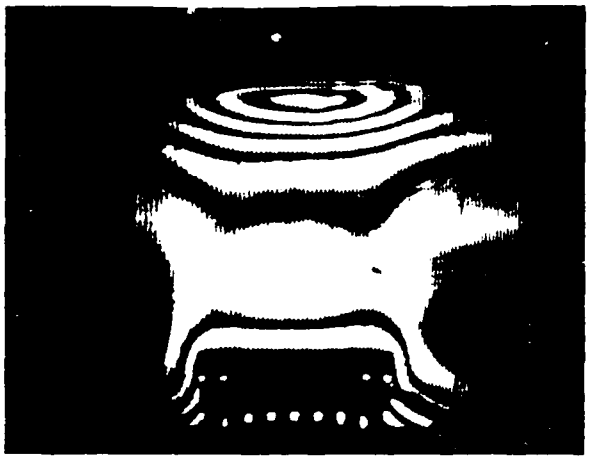

Fig. 3(a)

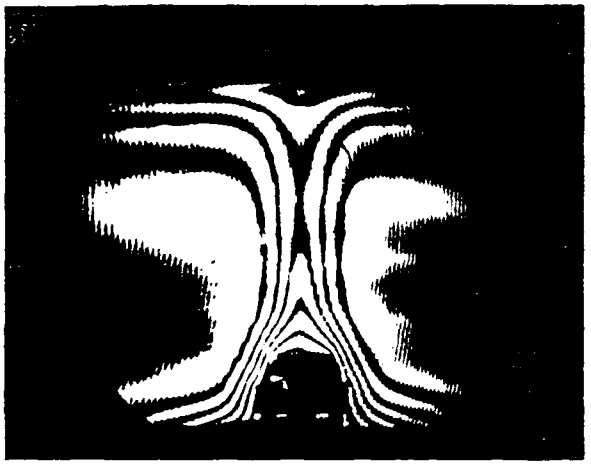

Fig. 3(b)

Fig. 3 Interferograms corresponding to orthogonal views through the volume of interest. (a) Broadside view of chip. (b) Longitudinal view of chip. The temperature is the same for both, $q = 4.45$W, $T_c = 226$°C.

described above by correlating the voltage-off holograms with the proper voltage-on holograms. Note that in Fig. 3, the broadside view can be used to determine the path of integration (for data inversion) for the longitudinal view.

Figure 4 shows the results obtained when the chip is placed in deionized water. The initial temperature of the water was 20.6°C whereas after applying the voltage it rose to 32.5°C. The dark semicircles on the bottom of the plate are bubbles that formed before recording. The fringe density is significantly increased due to the density of the water. The fringes beyond the plate are now clearly seen.

Figure 5 shows fringes obtained with the chip placed in air without the top plate. The dissipated energy is set the same as that for Fig. 3(*b*). The fringe patterns in the vicinity of the chip in Figs. 3(*b*) and 5 are nearly identical. The measured temperature of the chip in Fig. 5 is 5°C less than that for Fig. 3(*b*). Therefore, the effect of the upper plate, shown in Figs. 2 and 3, on the heat transfer rate is apparently small in this example.

The optical depth in Fig. 5 is nearly constant and the fringes approximate isotherms. The optical depth in Figs. 2, 3, and 4 changes as the upper plate forces the plume to spread laterally. The temperature decreases along these fringes as the optical depth increases. For example, the optical depth for fringes immediately to the right and the left of the chip in Fig. 2(*c*) is smaller than the optical depth for the fringes near the top plate. The temperature increase between the quiescent air temperature and the next fringe toward the chip is approximately 21°C. Away from the chip, if the optical depth is

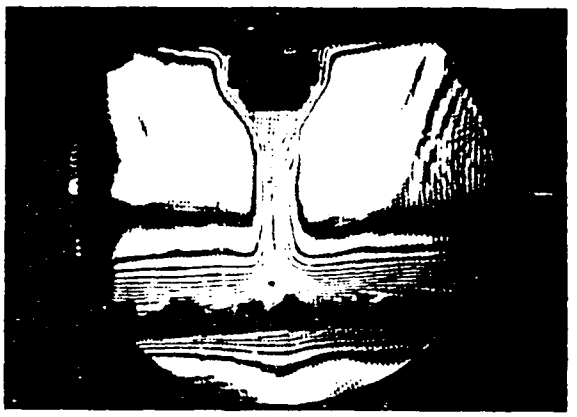

Fig. 4 Interferogram indicating heat transfer from the chip located in water, $q = 2.75$W, $T_c = 32.5$°C

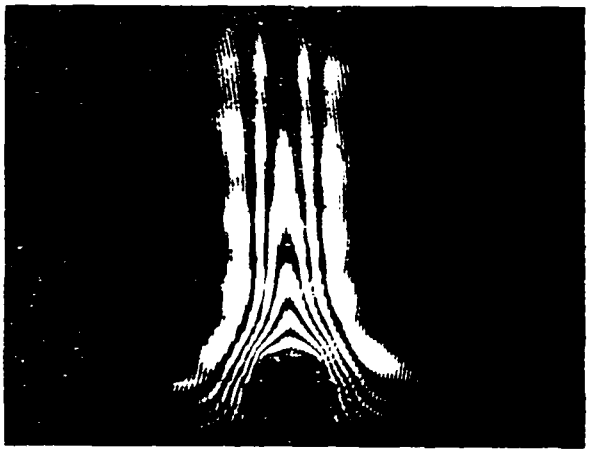

Fig. 5 Similar to Fig. 3(*b*) but without a top plate, $q = 4.45$W, $T_c = 221$°C

doubled, the temperature increase from the quiescent air temperature (toward the plate) is ~ 10.5 deg for the first fringe. If the optical depth is tripled, this temperature difference drops to less than 7°C. This implies that the interesting fringe patterns near the top in Figs. 2(*c*), 3(*a*), (*eb*), and 4 are caused by the combined effect of the temperature field and variable optical depth caused by the plate that blocks the otherwise vertical plume.

The heat transfer from the chip, for the holograms shown in Figs. 2 through 5, is compared with available data, and the results are given in Fig. 6. The empirical results of King (1932) are used for comparison. King's relation is widely used in heat transfer texts, e.g., Karlekar and Desmond (1982). The data reported by King are for a block with length L, width W, and height H. In this comparison, it is necessary to employ the same characteristic length used by King. The characteristic length used in calculating the Rayleigh number, $\mathrm{Ra} = g\beta(T_c - T_a)L_c^3/\nu\alpha$, is $L_c = (LH)/(L + H)$, where $L = 2.15$ cm is the length of the chip and $H = 0.8$ cm is the total height of the chip plus the socket. The thermophysical properties are calculated at the mean fluid temperature; the value of the thermal expansion coefficient, β, is selected at the ambient temperature. The ordinate of Fig. 6 is the dimensionless heat transfer coefficient; that is, the Nusselt number, $\mathrm{Nu} = \bar{h}L_c/k$, where $\bar{h} = (q/A)/(T_c - T_a)$ and A is the exposed area of the chip plus socket.

As seen from Fig. 2, natural convection can occur only at relatively high temperatures. The measured temperature and power dissipation are accurate to within 1 percent; however, there are geometrical complexities that are peculiar to the chip assembly. The Nusselt numbers in Fig. 6 are slightly higher than expected because of a simplified geometrical model when the entire heat loss is assumed to be from the surfaces of a 0.64

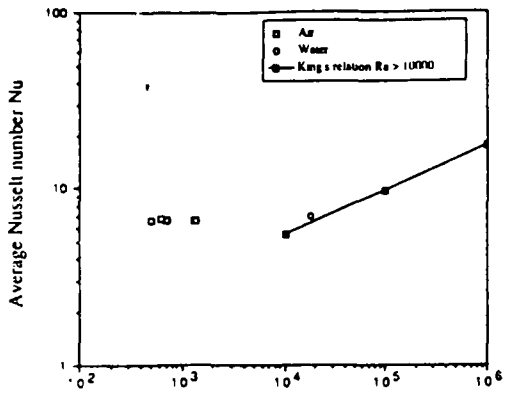

Fig. 6 Rayleigh number as a function of Nusselt number plotted using data from the results in Figs. 2-5. King's relation is also plotted for comparison.

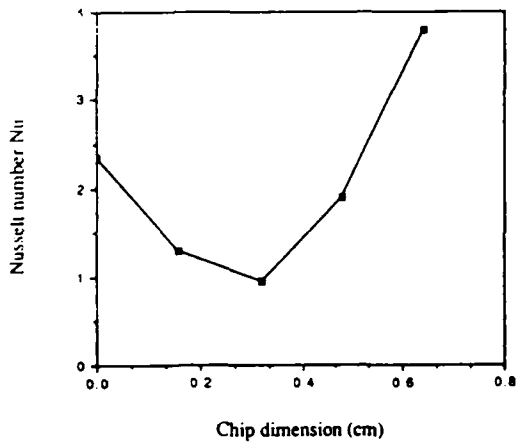

Fig. 7 Variation of the local Nusselt number over the chip surface

cm × 2.15cm × 0.8cm block. The King relation $\overline{Nu} = 0.55\ Ra^{0.25}$ (valid for $10^4 \le Ra \le 10^9$ according to Karlekar and Desmond, 1982) is plotted in Fig. 6 for comparison.

As seen in Fig. 2(*a*), there is no natural convection at Ra = 497. However, Fig. 2(*b*) shows that a plume appears at Ra = 710. The Nusselt number for the data in Fig. 6 is relatively insensitive to the Rayleigh number. This indicates that heat transfers by conduction while the contribution of convection is small. It is easy to show that conduction from any surface whose temperature is constant produces a constant value of h/k. The temperature field, when Ra is small, is governed by the Laplace equation, $\nabla^2\Theta = 0$, where $\Theta = (T - T_a)/(T_c - T_a)$. The value of Θ is 1 at the heated wall and 0 far away from the wall. Then, the quantity h/k is $-(\partial\Theta/\Theta\partial n)_{wall}$, which is independent of the wall temperature. Because h/k is constant everywhere on the surface of the chip, then the $\overline{Nu}$ is also a constant. Therefore, $\overline{Nu}$, as shown in Fig. 6, is constant in the absence of convective effects. The natural convection effect is small when $Ra < 10^4$ and $\overline{Nu}$ changes between 6.4 and 7.0. The Rayleigh number is a measure that indicates when the buoyancy effect becomes significant.

An accurate quantitative evaluation of local heat transfer from the top surface of a chip, using fringes shown in Figs. 2 and 3 is difficult because of the relatively large spacing between the fringes. The spacing between fringes is significantly smaller in Fig. 4, where water, instead of air, is used as the fluid. A detailed parametric study of the local heat transfer is beyond the scope of this paper. However, to demonstrate the concept, the local heat transfer coefficient at the top surface of the chip using the fringes in Fig. 3(*b*) is calculated. The optical path for Fig. 3(*b*) can be deduced from Fig. 3(*a*). The end effects in the optical path are neglected in the calculations. The method of calculation of the temperature along fringe lines is given by Vest (1979). The variation of the local Nusselt number, hL_c/k, in the spanwise direction over the chip surface is given in Fig. 7. The heat flux at the top surface is quite low compared to vertical surfaces. This can be observed from the fringe pattern where the spacing between fringes is quite small along the sides of the chip. The data are in qualitative agreement with those in Fig. 6; estimated error is ±20 percent.

Conclusions

Holographic interferometry using self-developing optical crystals is a convenient method for evaluating heat flux from small heated bodies. It can be used for flow visualization and for quantitative evaluation of the heat flux. In an established facility, photographic, or computer-acquired results can be produced in a few minutes. Although natural convection is employed for the work reported in this paper, this method can be used to study two-dimensional and even three-dimensional forced convection. Also, many transient problems can be accommodated without major modification. For these, a cw laser and an appropriate shutter would suffice for relatively slow effects. For fast transients, a pulsed laser with short (nanoseconds) pulses and high repetition rates would be required.

Acknowledgments

This work was partially supported by the U.S. Army Research Office under grant DAAL03-86-K0149 and by the Texas Advanced Research Program under grant 1758.

References

Ashkin, A., Boyd, G. D., Dziedzic, J. M., Smith, R. G., Ballman, A. A., Levinstein, J. J., and Nassau, K., 1966, "Optically-Induced Refractive Index Inhomogeneities in $LiNbO_3$ and $LiTaO_3$," *Appl. Phys. Letters*, Vol. 9, pp. 72-74.

Chen, F. S., 1967, "A Laser Induced Inhomogeneity of Refractive Indices in KTN," *J. Appl. Phys.*, Vol. 38, pp. 3418-3420.

Chen, F. S., LaMacchia, J. T., and Fraser, D. B., 1968, "Holographic Storage in Lithium Niobate," *Appl. Phys. Letters*, Vol. 13, pp. 223-225.

Feinberg, J., Heiman, D., Tanguay, A. R., and Hellwarth, R. W., 1980, "Photorefractive Effects and Light-Induced Charge Migration in Barium Titanate," *J. Appl. Phys.*, Vol. 51, pp. 1297-1305.

Glass, A. M., 1978, "The Photorefractive Effect," *Optical Engineering*, Vol. 17, pp. 470-479.

Glass, A. M., Johnson, A. M., Olson, D. H., Simpson, W., and Ballman, A. A., 1984, "Four-wave Mixing in Semi-Insulating InP and GaAs Using the Photorefractive Effect," *Appl. Phys. Letters*, Vol. 44, pp. 948-950.

Hariharan, P., 1984, *Optical Holography—Principles, Techniques and Applications*, Cambridge University Press, Cambridge, MA.

Huignard, J. P., and Herriau, J. P., 1977, "Real-Time Double-Exposure Interferometry With $Bi_{12}SiO_{20}$ Crystals in Transverse Electrooptic Configuration," *Appl. Opt.*, Vol. 16, pp. 1807-1809.

Huignard, J. P., Herriau, J. P., and Valentin, T., 1977, "Time Average Holographic Interferometry With Photoconductive Electrooptic $Bi_{12}SiO_{20}$ Crystals," *Appl. Opt.*, Vol. 16, pp. 2796-2798.

Huignard, J. P., and Micheron, F., 1976, "High-Sensitivity Read-Write Volume Holographic Storage in $Bi_{12}SiO_{20}$ and $Bi_{12}GeO_{20}$ Crystals," *Appl. Phys. Letters*, Vol. 29, pp. 591-593.

Ja, Y. H., 1982, "Real-Time Double-Exposure Holographic Interferometry In Four-Wave Mixing With Photorefractive $Bi_{12}GeO_{20}$ Crystals," *Appl. Opt.*, Vol. 21, pp. 3230-3231.

Karlekar, B. V., and Desmond, R. M., 1982, *Heat Transfer*, West Publishing Co., St. Paul, Minn.

King, W. J., 1932, "The Basic Laws and Data of Heat Transmission," *Mechanical Engineering*, Vol. 54, p. 347.

Magnusson, R., Mitchell III, J. H., Black, T. D., and Wilson, D. R., 1987, "Holographic Interferometry Using Iron-Doped Lithium Niobate," *Appl. Phys. Letters*, Vol. 51, pp. 81-82.

Marrakchi, A., Herriau, J. P., and Huignard, J. P., 1982, "Real-Time Holographic Interferometry With Photorefractive $Bi_{12}SiO_{20}$ Crystals," *Proc. S.P.I.E.*, Vol. 353, pp. 24-28.

Thaxter, J. B., 1969, "Electrical Control of Holographic Storage in Strontium-Barium Niobate," *Appl. Phys. Letters*, Vol. 15, pp. 210-212.

Vest, C. M., 1979, *Holographic Interferometry*, Wiley, New York.